This dissertation has been microfilmed exactly as received

65–4892

PARK, Jr., Efton Lilborn, 1936–
NUCLEATE AND FILM BOILING HEAT TRANSFER TO METHANE AND NITROGEN FROM ATMOSPHERIC PRESSURE TO THE CRITICAL PRESSURE.

The University of Oklahoma, Ph.D., 1965
Engineering, chemical

University Microfilms, Inc., Ann Arbor, Michigan

Downloaded from SHAREOK. Persistent Handle URL: https://hdl.handle.net/11244/1833



THE UNIVERSITY OF OKLAHOMA

GRADUATE COLLEGE

NUCLEATE AND FILM BOILING HEAT TRANSFER TO METHANE AND NITROGEN FROM ATMOSPHERIC PRESSURE TO THE CRITICAL PRESSURE

A DISSERTATION

SUBMITTED TO THE GRADUATE FACULTY

in partial fulfillment of the requirements for the

degree of

DOCTOR OF PHILOSOPHY

BY

EFTON L. PARK, JR.

Norman, Oklahoma

1965

NUCLEATE AND FILM BOILING HEAT TRANSFER TO METHANE

AND NITROGEN FROM ATMOSPHERIC PRESSURE

TO THE CRITICAL PRESSURE

APPROVED BY

C. M. Sliepcevich

Raymond O. Heston

[illegible]

D. G. Harden

F. Mark Townsend

DISSERTATION COMMITTEE

ABSTRACT

Nucleate boiling heat transfer, film boiling heat transfer, and convective heat transfer (at pressures greater than the critical pressure) studies were conducted on a gold surface for methane and nitrogen.

The data obtained were compared with equations which are commonly used to predict boiling heat transfer behavior for cryogenic fluids. The conclusion was drawn that the equations which were compared to the data in both the film and nucleate boiling regions are of little value except as rough approximations.

The film boiling heat flux for a specific temperature difference was found to decrease rapidly with increasing pressure at reduced pressures greater than 0.9. Below a reduced pressure of 0.8 the effect of pressure on the film boiling heat flux was found to depend on the magnitude of the temperature difference. For low temperature differences the flux at a given temperature difference decreases with increasing pressure. At high temperature differences the flux at a specific temperature difference was found to increase with increasing pressure.

The convective heat transfer coefficient exceeds the coefficient found in the film boiling region over the limited

pressure range covered.

A theoretical equation which correlates the available data on critical temperature differences for liquids, which follow the law of corresponding states, has been derived and discussed.

ACKNOWLEDGMENTS

The author wishes to express his thanks to the following people and organizations for their help which made the completion of this investigation possible.

Dr. C. M. Sliepcevich for his suggestions and advice during the course of this investigation.

Dr. F. M. Townsend and Dr. Frank Canfield who were willing to listen and offer advice.

Dr. C. P. Colver who offered many helpful suggestions during this investigation.

Dr. Darrel Williams who helped when repairs were needed on the electrical apparatus.

Frank MaGinnis of The Research Instrument Company whose contribution was greater than the heat transfer element design and fabrication for which he was hired.

Tom Sciance for his help in collecting data.

Conch Methane Services who provided financial support for this investigation.

Continental Oil Company who furnished the liquid methane used in this investigation.

My wife Janice, whose contributions to this work are too numerous to list.

TABLE OF CONTENTS

		Page
LIST OF ILLUSTRATIONS		vii
Chapter		
I.	INTRODUCTION	1
II.	PREVIOUS WORK	5
III.	EXPERIMENTAL EQUIPMENT	19
IV.	EXPERIMENTAL PROCEDURE	25
V.	DERIVATION OF EQUATION FOR CRITICAL TEMPERATURE DIFFERENCES	29
VI.	RESULTS AND DISCUSSION	33
VII.	DISCUSSION OF ERRORS	61
VIII.	CONCLUSIONS	64
NOMENCLATURE		66
LITERATURE CITED		68
APPENDICES		
A.	EXPERIMENTAL DATA	73
B.	SAMPLE CALCULATIONS	103
C.	DISCUSSION OF THE EFFECT OF END LOSSES FROM THE HEAT TRANSFER ELEMENT	106
D.	CALIBRATION OF THERMOCOUPLES	109
E.	CALIBRATION CURVE FOR PRESSURE GAUGE	111
F.	CALCULATED PHYSICAL PROPERTIES	113

LIST OF ILLUSTRATIONS

Figure		Page
1.	A Typical Boiling Heat Transfer Curve	2
2.	Pressure Volume Diagram From van der Waal's Equation	15
3.	Heat Transfer Element	20
4.	Pressure Vessel	23
5.	Variation of ϵ With Reduced Temperature	31
6.	Comparison of ΔT at the Top of the Heat Transfer Element With ΔT at the Bottom of the Element	35
7.	Comparison of Experimental Data for Nucleate Boiling Heat Transfer With Correlating Equations	36
8.	ΔT Versus Heat Flux for Methane Nucleate Boiling	38
9.	ΔT Versus Heat Flux for Nitrogen Nucleate Boiling	39
10.	Comparison of the Critical Heat Flux Data With Previous Data	42
11.	Comparison of the Critical Heat Flux With Predicted Values	43
12.	Comparison of the Data for Critical Temperature Differences With Frederking's Predicted Curve	45
13.	Variation of ϵ With Reduced Temperature for This Investigation	46
14.	Comparison of Available Data With Equation 15	48
15.	Comparison of Data for Liquids Which Do Not Follow the Law of Corresponding States With Equation 15	49
16.	ΔT Versus Heat Flux for Nitrogen Film Boiling	51

Figure Page

17. ΔT Versus Heat Flux for Methane Film Boiling . . 52

18. ΔT Versus Heat Flux for Oxygen Film Boiling . . . 53

19. Comparison of Methane Film Boiling Data With Equation 12 55

20. Comparison of Nitrogen Film Boiling Data With Equation 12 56

21. ΔT Versus Heat Flux for Convective Heat Transfer 58

22. ΔT Versus Heat Flux for Convective Heat Transfer 59

NUCLEATE AND FILM BOILING HEAT TRANSFER TO METHANE AND NITROGEN FROM ATMOSPHERIC PRESSURE TO THE CRITICAL PRESSURE

CHAPTER I

INTRODUCTION

Renewed interest in the field of boiling heat transfer has occurred in the last ten years due to recent technological developments in nuclear reactors, rocket engines and cryogenic equipment.

The entire boiling curve and the different boiling regimes were first discussed by Nukiyama (43) in 1934. It was found that boiling heat transfer could be divided into the four distinct regions shown in Figure 1. The four types of boiling heat transfer can best be understood by considering a heat transfer surface in contact with a saturated liquid. As the surface temperature is raised slightly above the liquid saturation temperature, convective currents circulate the liquid and evaporation occurs at the free surface of the liquid. If the surface temperature is increased further, the nucleate boiling region is entered. Bubbles begin to form at specific points on the surface called nuclei. With increasing surface temperature more nuclei appear or become

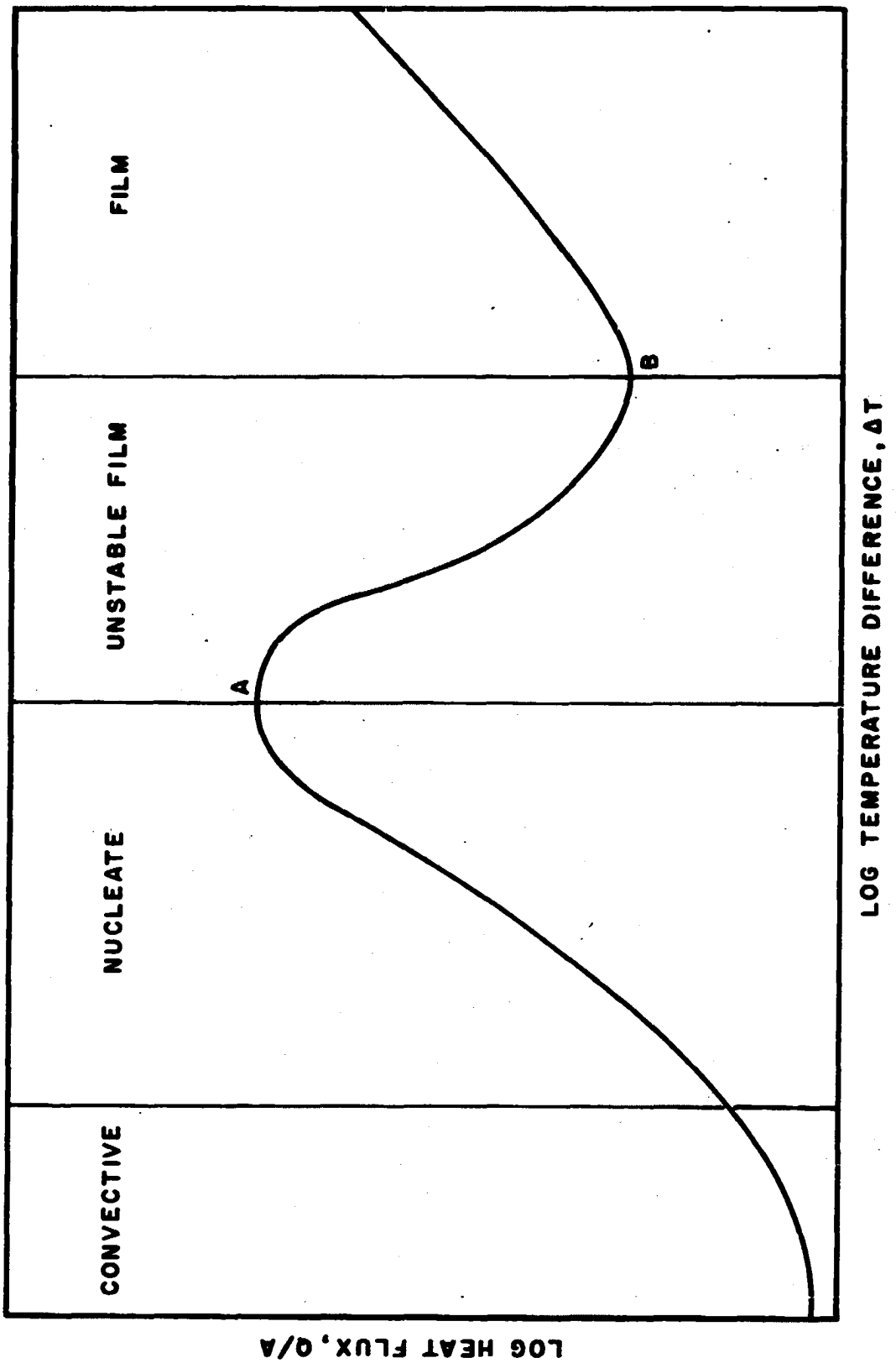

Figure 1. A Typical Boiling Heat Transfer Curve

active. The nucleate boiling region is of special interest because of the high heat fluxes which are obtained with relatively small driving forces. As the surface temperature is increased further, the bubbles which are forming suddenly combine to form a film of vapor over the heat transfer surface. This condition corresponds to point A in Figure 1. Point A is known as the critical heat flux or burnout point. Beyond point A the vapor film forms and collapses rapidly. The added resistance due to the film formation causes the heat transfer rate to drop quickly. This unstable film region continues until point B (Liedenfrost Point) is reached. At point B the film of vapor becomes stable in the sense that it does not form and collapse as in the unstable film boiling region. However, the film surface is still in violent agitation. The film boiling region, once considered to be only an academic curiosity, is rapidly becoming an important field of heat transfer because of the data needed for design of cryogenic equipment.

Recently there have been several articles published (5,10,19,20,36) which suggest that the behavior at point A of similar substances can be correlated using the reduced properties of the liquids (i.e., T/T_c or P/P_c). To date, experimental verification of this theory has been restricted to correlations of burnout points for organic compounds and water. Since water and organic compounds have complicated molecules which cannot be considered similar, verification of this theory depends on obtaining data on substances which can

be considered similar.

Data in the film boiling region over a range of pressures appears to be restricted to one set of oxygen data (1). More data are needed to check the theoretical equations which are available and to describe fully the effect of pressure on film boiling heat transfer.

This study was initiated to provide data in the areas described above and to provide design data for methane and nitrogen boiling heat transfer.

CHAPTER II

PREVIOUS WORK

In recent years a large number of publications have been concerned with investigation of the sites (nuclei) on which bubbles form in the nucleate boiling region. Corty and Foust (12) found that the position and the slope of the boiling curve vary with roughness. It was noted that while the temperature difference at a given heat flux decreases with roughness the maximum temperature difference which can be reached before nucleate boiling is initiated increases with roughness. Past boiling history of the surface was also found to play an important part in the initiation of nucleate boiling. Corty and Foust explained the above phenomena by a vapor entrapment model. It was postulated that surface pits and scratches which were capable of entrapping vapor as the bubbles left the surface were active sites.

Clark, Strenge, and Westwater (11) using high speed photography confirmed that pits and scratches were in fact nucleation sites. It was found that pits with diameters between 0.0003 inches and 0.003 inches were the most active sites although other surface defects such as scratches, and in one case foreign material, also acted as active nucleation

sites.

Kurihara and Myers (34) confirmed Corty and Foust's work and found that aging the surface in the liquid to be boiled allowed reproducible runs to be obtained. It was postulated that this aging allowed any excess inert gas entrapped on the surface to diffuse into the liquid leaving a surface which could be reproduced.

Bankoff (2,3) in recent papers discusses the effect of surface geometry and liquid-solid contact angle on the ability of a cavity to become an active site. He also presented an approximate theory for predicting the superheat required to initiate bubble formation from an active cavity.

Denny (13) investigated nucleate boiling of carbon tetrachloride from well defined artificial pits of varying geometries and found the most active nuclei were steep walled cavities with a depth to diameter ratio greater than one. Fouling which affected the internal dimensions of the site, the local surface roughness of the site, and the surface chemistry of the site were also found to be important variables which affect site activity.

Griffith and Wallis (24) determined that the cavity geometry is important in two ways. The mouth diameter determines the superheat required to initiate boiling; the cavity shape determines the stability of the site after boiling is initiated.

Gaertner and Westwater (22) found that the number of active sites can be as high as 1130 sites per square inch at

heat fluxes which were below the critical heat flux, where the maximum site concentration occurs. Their excellent study also disproved the theory held by earlier workers (28,40) that the site population increases linearly with increasing heat flux.

At present pits and scratches which are capable of trapping vapor are accepted as the nucleation sites as postulated by the work reviewed above. However, the mechanism which accounts for the high heat transfer rate found in nucleate boiling has not been definitely established. Since knowledge of the mechanism of nucleate boiling heat transfer is a prerequisite to formulation of a generalized correlation, some of the commonly proposed mechanisms will be briefly discussed.

Mechanism 1: Microconvection in the Sublayer

This mechanism was the most widely accepted mechanism by early workers (28,40). The high heat transfer rates are postulated to be due to large convective velocities in the superheated sublayer of the liquid. These large convective velocities are caused by the growth and collapse of the bubbles. As was pointed out by Forster and Grief (17), if mechanism 1 is correct the heat flux should be strongly dependent on the temperature difference ($T_{wall} - T_{liquid}$); however, experimental investigations of subcooled liquids do not show this strong dependence.

Mechanism 2: Latent Heat Transport by Bubbles

It is postulated that as a bubble grows it absorbs latent heat which is returned to the bulk liquid when the bubble collapses. It has been shown (48) that this mechanism can only account for a small percentage of the total heat which is transfered.

Mechanism 3: Vapor-Liquid Exchange Action

This mechanism which was first discussed by Forster and Grief (17) assumes that as the bubble grows superheated liquid is forced from the superheated liquid layer into the bulk liquid and that upon bubble detachment, cool liquid rushes in to fill the void left by the departing bubble.

Mechanism 4: Mass Transfer Through the Bubble

It is postulated that as the bubble grows on the surface the inside of the bubble is exposed to a micro-layer of liquid which wets the surface. This liquid layer evaporates into the interior of the bubble and condenses on the bubble top where it gives up the latent heat of vaporization.

In a recent investigation, Moore and Mesler (42) found that the surface temperature drops 20 to 30°F in about 2 milliseconds during nucleate boiling. This surface temperature fluctuation, which had not been previously measured, was investigated by using a specially designed thermocouple which was an integral part of the heat transfer surface. There is nothing in mechanism 1 or 3 which can account for this large surface temperature drop. Mechanism 3 postulates

that cool water rushes to the heater surface upon bubble departure; however as was pointed out by Moore and Mesler, the large temperature fluctuations that were observed would require liquid which was supercooled to be present. Moore and Mesler note in their paper that mechanism 2 is consistent with their experimental work.

Gaertner's (21) excellent photographic study pointed out that there are three and possibly four distinct regions in nucleate boiling. The regions (discrete bubble region, first transition region, vapor mushroom region, and second transition region) were characterized by the mode of vapor formation.

In view of the previous work, it appears that a combination of several mechanisms is required to explain the nucleate boiling region.

Several correlating equations (17,18,35,41) have been proposed for the nucleate boiling region; however, at this time no general equation describing the nucleate boiling region has been found. This absence is, probably, due to two factors. One, the surface characteristics have been neglected in all the published correlations. Two, the present correlations are all based on either mechanism 1 or 3. It is unlikely that a general equation describing nucleate boiling will be discovered until the mechanism of nucleate boiling is understood and the heat transfer surface can be characterized.

Technologically the most important point on the boiling curve is the burnout point. In the nucleate boiling region heat transfer coefficients of 1000 Btu/°F-ft^2 are not uncommon; however, upon entry into the film boiling region the heat transfer coefficient may drop by a factor of twenty or more. In addition to the undesirable heat transfer which is common to the film boiling region, the heat transfer surface can be melted because of the poor heat transfer away from the surface. Because of these factors, a reliable equation which can be used to predict critical heat fluxes is of primary interest to the investigators studying boiling heat transfer. At present, there is no general equation which will predict the burnout point. There have, however, been several equations published which fit a part of the data available.

Rohsenow and Griffith (49) propose the critical heat flux correlation given by equation 1. Their semi-empirical equation is based on data for organic liquids and water.

$$\frac{(Q/A)_{max}}{\rho_v L} = 143 \left(\frac{\rho_L - \rho_v}{\rho_v} \right)^{0.6} \text{ ft/hr} \qquad (1)$$

Where: L is the latent heat of vaporization

ρ_v is the vapor density.

ρ_L is the liquid density.

Kutateladze (33) by use of dimensional analysis developed the burnout correlation given by equation 2.

$$\frac{(Q/A)_{max}}{\rho_v L} = 0.16 \left[\sigma g \left(\frac{\rho_L - \rho_v}{\rho_v^2} \right) g_c \right]^{1/4} \qquad (2)$$

Where: σ is the surface tension.

g is acceleration due to gravity.

Zuber (53) based his correlation on the limiting stability of two phase flow. The resulting correlation is given by equation 3.

$$\frac{(Q/A)_{max}}{\rho_v L} = \frac{\pi}{24} \left[\sigma g \left(\frac{\rho_L - \rho_v}{\rho_v^2} \right) g_c \right]^{1/4} \left[\frac{\rho_L}{\rho_L + \rho_v} \right]^{1/2} \qquad (3)$$

Cichelli and Bonilla (10) found that they could empirically correlate their experimental data for a large number of organic liquids by equation 4.

$$\frac{(Q/A)_{max}}{P_r} = \alpha \, f(P_r) \qquad (4)$$

Where: P_r is the reduced pressure.

α is equal to 1 for clean surfaces.

α is equal to 1.15 for dirty surfaces.

Addoms (40) suggested the empirically determined correlation given by equation 5.

$$\frac{(Q/A)_{max}}{\rho_v L \left(\frac{K_L g}{\rho_L C_L} \right)^{1/3}} = f \left(\frac{\rho_L - \rho_v}{\rho_v} \right) \qquad (5)$$

Where: K is the thermal conductivity.

C is the specific heat.

None of the equations given above can adequately correlate all of the experimental data that are available. Use of these equations can in many cases predict values which are several hundred per cent in error. This discrepancy is not surprising as none of the correlations consider surface effects. Upon closer study of the equations given above, it becomes apparent that the critical heat flux is a function only of the thermodynamic properties of the fluid in all cases. Therefore, for liquids, which are thermodynamically similar and for boiling on the same surface it is probable that a correlation using reduced properties of the liquids can be found. Lienhard and Schrock (36); Borishansky, Novikov, and Kutateladze (5); Frederking (19); and Cichelli and Bonilla (see equation 4) have published work which support this theory.

Lienhard and Schrock used equation 3 as a basis for their work. By manipulating the Clausius Clapeyron equation, the expression for van der Waal's reduced volume, the defining equation for the parachor, and equation 3 they obtained equation 6.

$$\frac{(Q/A)_{max}}{\lambda_{max}} = f\left(P_r,\ T_r,\ \rho_{Lr},\ \rho_{vr},\ \left.\frac{dP_r}{dT_r}\right|_{sat}\right) \qquad (6)$$

Where: ϕ is the parachor.

M is molecular weight.

$$\lambda_{max} = \frac{\pi}{24}\left[\sqrt[4]{g} \cdot P_c \cdot \frac{\psi}{M}\left(\frac{8\ M\ P_c}{3\ R\ T_c}\right)^{3/4}\right]$$

Borishanski and coworkers discuss the theory of thermodynamic similarity as applied to the critical heat flux. They also propose equation 7 as a correlation for critical heat flux.

$$\frac{(Q/A)_{max}\sqrt{M}}{P_c\sqrt{T_c}} = f(P_r) \qquad (7)$$

Equations 6 and 7 were tested with data obtained by boiling organic liquids and water. Equation 6 was tested with data obtained on the same surface; however, the data used to test equation 7 came from several sources. While the work cited above is interesting and tends to support the thermodynamic similarity theory, definite confirmation of the theory depends on obtaining data for liquids which follow the law of corresponding states to a high degree of accuracy such as argon, krypton, xenon, nitrogen, methane, oxygen, or carbon monoxide (25).

Frederking (19,20) developed an interesting equation for prediction of the temperature difference at the burnout point based on an estimate of the possible metastable states in which a two phase system can exist. For a given pressure, the maximum superheat occurs at the minimum of the metastable isotherms on a P-V diagram. Therefore, with a surface free of defects, a liquid which obeys van der Waal's equation

should attain a liquid superheat corresponding to ΔT_{vw} shown in Figure 2. Differentiating van der Waal's equation,

$$P_r = \left[\frac{8T_r}{(3V_r - 1)} \right] - \left[\frac{3}{V_r^2} \right]$$

and minimizing with respect to V_r, gives an expression (equation 8) for the reduced maximum temperature difference that can be expected.

$$\Delta T_r = \frac{\Delta T_{vw}}{T_c} = T_r^* - T_{r_{sat}} \tag{8}$$

$$T_r^* = \frac{(3V_r - 1)^2}{4V_r^3}$$

Since it would require a perfectly smooth surface to attain a superheat of ΔT_{vw}, Frederking suggests that the degree of metastability attained be defined as,

$$\epsilon = \frac{\Delta T_{bo}}{\Delta T_{vw}} = \frac{\text{temperature difference in actual system}}{\text{theoretical temperature difference}} \tag{8a}$$

As a first approximation Frederking assumed that the degree of metastability, ϵ, was equal to 0.5. As was pointed out by Frederking, this work is highly idealized as van der Waal's equation and the law of corresponding states have been assumed; however, the theory presented here should be helpful in future heat transfer investigations.

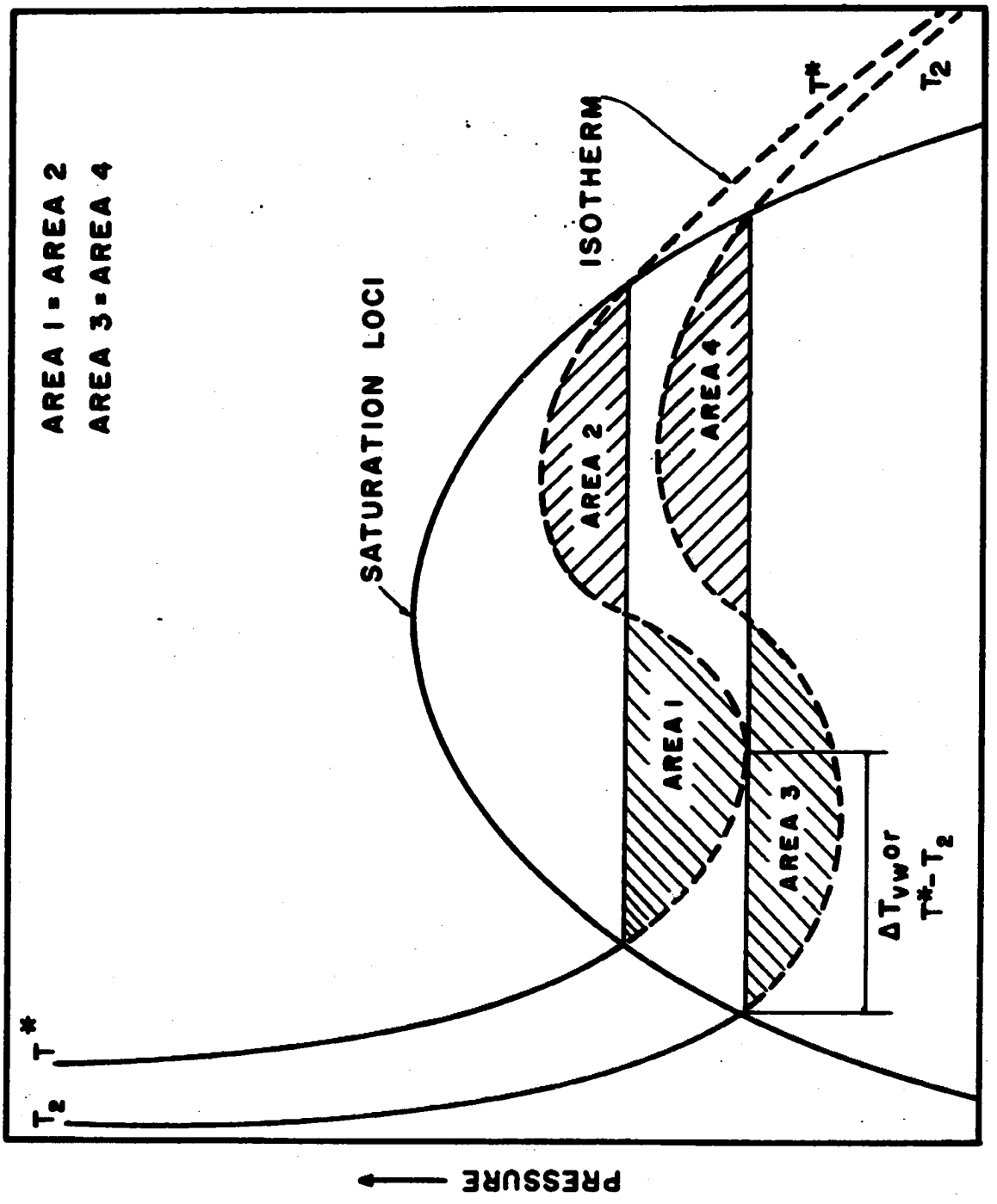

Figure 2. Pressure Volume Diagram From van der Waal's Equation

The transition region (unstable film boiling) has received little attention for two reasons. First, it is the most difficult region to study. The use of electric heaters is difficult because of the instability of the heaters in the unstable film boiling region. Therefore, the investigator must employ a hot liquid or a condensing vapor as a heat source. Second, a study of the transition region has no practical use as industrial equipment cannot be designed which will operate in this region. At present no work of a theoretical nature has been published in the area of unstable film boiling; and, very little experimental data are available. Westwater (15) has summarized the experimental data which are available.

The film boiling region has received only a fraction of the attention that the nucleate boiling region has. The first theoretical equation for the film boiling region was proposed by Bromley (7). Bromley suggested that an equation similar to Nusselt's film condensation equation with modifications in the coefficient and the physical properties would characterize film boiling. The final form of the equation for horizontal tubes is given by equation 9.

$$h = \text{const.} \left[\frac{K_V^3 \rho_V (\rho_L - \rho_V) I g}{D \mu_V \Delta T} \right]^{1/4} \qquad (9)$$

Where μ_V is the viscosity of the vapor and h is the heat transfer coefficient due to convection. The constant was determined empirically to be 0.62. The theoretical

coefficient is 0.512 for a stagnant liquid around the vapor and 0.724 for liquid moving at the same velocity as the vapor. Bromley suggests that the radiation heat transfer coefficient should be determined by assuming parallel plates and adding the contribution to h at high temperatures where radiation is significant. Bromley's equation has been found to fit experimental data over a limited range of diameters. Small diameter heaters approach the film thickness which is not allowed for in Bromley's derivation, and large diameters approach a flat plate which according to equation 9 has a zero heat transfer coefficient. Banchero, Barker and Boll (1) in their study of liquid oxygen suggest that the diameter range where Bromley's equation is valid is between diameters of 0.069 and 0.127 inches. These authors found equation 10 correlated their data for oxygen for a range of diameters from 0.025 to 0.75 inches.

$$h = a\left(\frac{1}{D} + C\right)\left[\frac{K_V^3\,\rho_V(\rho_L - \rho_V)gL}{\Delta T\,\mu_V}\right]^{1/4} \qquad (10)$$

where a is a temperature dependent function and C is equal to 36.5 in^{-1}.

In recent years, several authors have developed correlations for film boiling on flat horizontal surfaces (4,8,9,27) using the concept of Taylor instability. If a liquid lies above a vapor, Taylor instability will develop; that is, waves will form at the interface and rupture will occur allowing vapor to rise as bubbles. The wave length

of the smallest wave which can form at the surface is given by equation 11

$$\lambda_c = 2\pi \left[\frac{g_c \sigma}{g(\rho_L - \rho_v)} \right]^{1/2} \qquad (11)$$

Recently Breen and Westwater (6) have extended the Taylor instability theory to film boiling on horizontal cylinders. Their final equation is given below.

$$\frac{h \lambda_c^{1/4}}{F} = h \left[\frac{\lambda_c \mu_v \Delta T}{K_v^3 \rho_v (\rho_L - \rho_v) g L} \right]^{1/4} = 0.59 + 0.069 \left(\frac{\lambda_c}{D} \right) \qquad (12)$$

Generality is claimed for equation 12 on the basis of data on several substances at atmospheric pressure and one set of data on oxygen (1) at a series of pressures. It will be shown later in this work that equation 12 is not general.

CHAPTER III

EXPERIMENTAL EQUIPMENT

The experimental equipment used in this work consisted of five basic elements, a heat transfer element, a power source, a pressure vessel, a gauge to measure pressure, and a potentiometer to measure temperatures.

The object of the heat transfer element design was to develop a simple heater for which end effects could be neglected (see Appendix C) and which could withstand the thermal shock of going through the burnout point and film boiling temperature differences of 1000°F. The final design (see Figure 3) consisted of a 0.44 inch diameter inner core of boron nitride on which 26 gauge tungsten wire had been wound in grooves cut in the core. There were 36 grooves per inch cut to a depth of 0.022 inches. The ends of the tungsten wire were held by taps on 1/8 inch diameter screws which were screwed into the core. The screws also acted as power leads for the resistance winding. The inner core was then cemented into a 2 1/32 inch long copper cylinder. The O.D. was 0.65 inches and the I.D. was 0.5 inches. The cement used was W. T. Bean, type H cement. Three slots 120 degrees apart were then milled one half the length of the copper tube

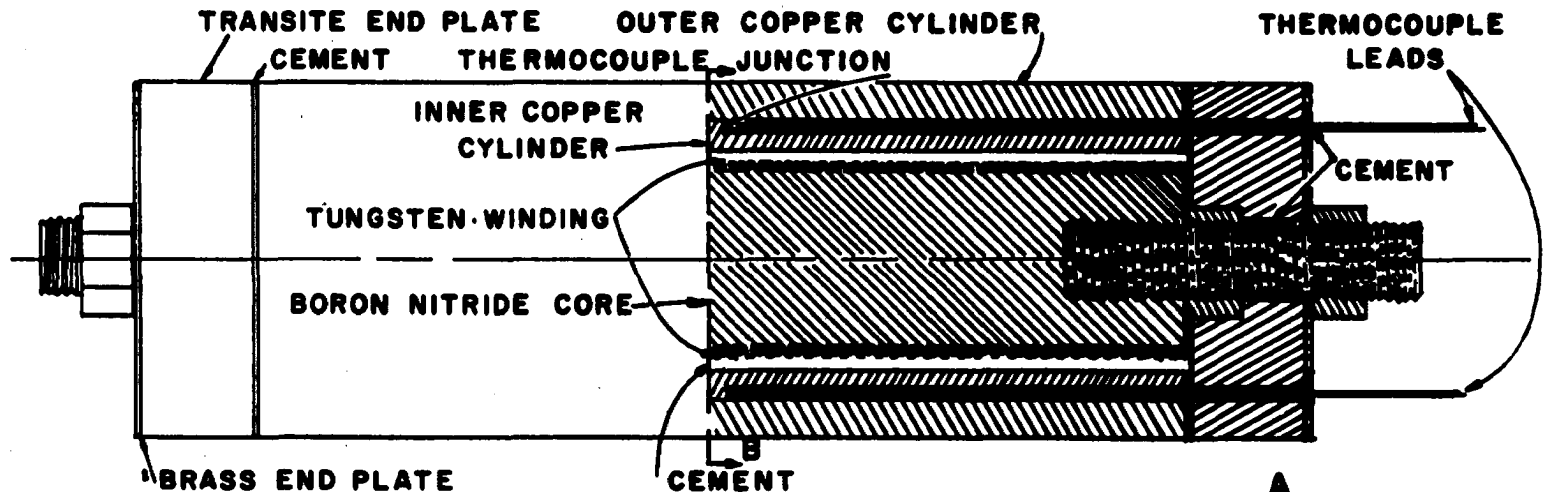

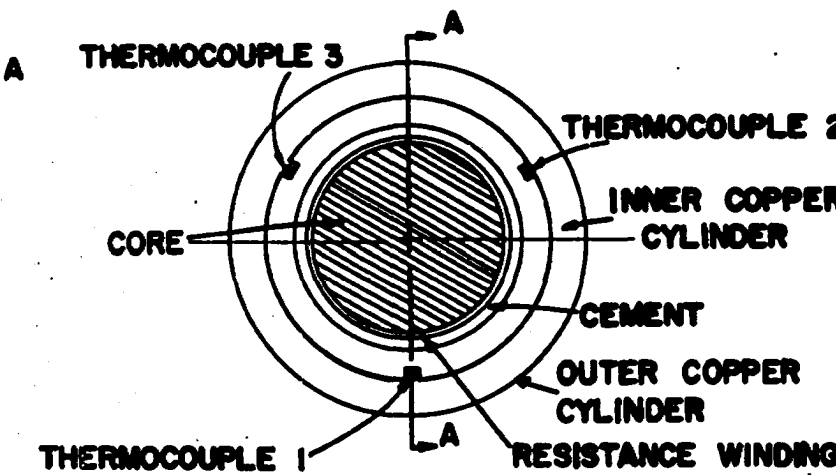

THERMOCOUPLE LOCATION IN HEATER

SECTION B-B

Figure 3. Heat Transfer Element

to a depth of 0.022 inches. Three 32 gauge iron-constantan thermocouples were silver soldered in the ends of the slots. The thermocouple wires were then cemented in place. This entire assembly was then placed inside a 0.8022 inch cylinder by shrink fitting. This construction assured good thermal contact between the two metal surfaces.

End plates made of transite were then cemented to the ends of the heater assembly to minimize heat losses.

Brass plates were then soft soldered to the screws which acted as power leads; and, number 12 copper wire was silver soldered to the brass plates to provide power leads to the heat transfer element.

Upon testing the element in liquid nitrogen, an oxide coating was observed to form on the heat transfer surface. (This coating was probably due to the oxygen contained in the liquid nitrogen). Since a reproducible surface was essential to this investigation, the heat transfer surface was gold plated at 0.2 amp. and 1.5 volts for thirty minutes with a cathode to anode ratio of 7. There was no visual deposit formed on the gold surface when the heat transfer element was tested again in liquid nitrogen.

The heat transfer element was powered by two model MA28-125 power sources which were connected in series. The range of control of the power source was from 18 to 72 volts with a maximum amperage of 125. To obtain the control needed for this investigation, a variable resistance made of 20 feet of number 10 nichrome wire was connected in series with the

power source. This resistance allowed the voltage to be varied between 2 and 72 volts.

The heat dissipated by the heat transfer element was determined by measuring the current flow and the voltage drop across the heat transfer element. The amperage was measured with a Simpson d.c. ammeter. The amperage could be measured accurately to ± 0.25 amps. The potential drop across the heater was measured using two d.c. Simpson voltmeters. One meter was used to measure the range 0 to 25 volts; the other was used in the range of 25 to 72 volts. The voltage measurements in the low range were accurate to ± 0.5 volts. The accuracy in the upper range was ± 2.0 volt.

The pressure vessel was a standard one liter autoclave (see Figure 4) with a confined gasket type closure. The inside diameter of the vessel was 3 inches; and, the depth of the vessel from the closure was 9 3/8 inches. Power and thermocouple leads entered the autoclave through two Conax electrical lead sealing glands. The pressure of the system was controlled by regulating the flow of liquid nitrogen through an internal condensing coil. The condensing coil was made of 10 feet of 1/4 inch stainless steel tubing. The tubing was coiled in such a manner that it extended only 2 1/2 inches from the closure of the pressure vessel. To minimize heat losses to the atmosphere the entire autoclave was surrounded by two feet of pearlite.

The system pressure was determined with a Heise bourdon tube pressure gauge. The 16 inch dial was graduated

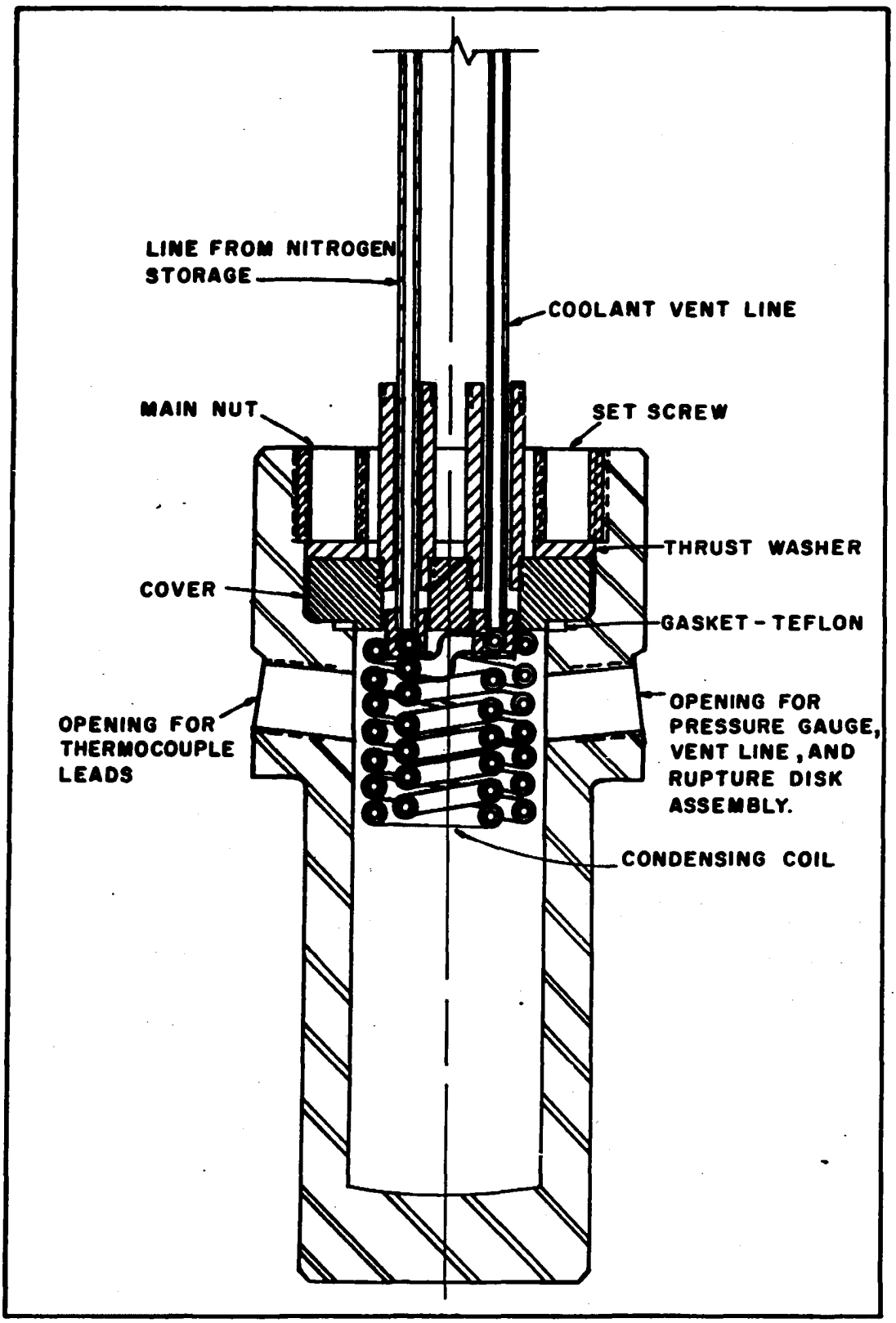

Figure 4. Pressure Vessel

from 0 to 1000 pounds per square inch in increments of one pound per square inch. An Ashcroft dead weight tester was used to calibrate the pressure gauge (see Appendix E). It was found that the pressure could be determined with an accuracy of ± one pound per square inch.

The temperatures were measured using a Leeds and Northrup portable precision potentiometer (number 8662). Millivolt readings below 15 millivolts could be read accurately to ± 0.005 millivolts. Above 15 millivolts the readings could be read with an accuracy of ± 0.025 millivolts. The thermocouples used in this investigation were calibrated using a platinum resistance thermometer (see Appendix D).

The cooling nitrogen was stored in Linde LS110 dewars which had been modified to give a working pressure of 235 pounds per square inch gauge. This arrangement provided sufficient driving force to the cooling nitrogen so that the system pressure could be controlled easily.

CHAPTER IV

EXPERIMENTAL PROCEDURE

Because surface effects can have an extreme effect on the heat flux in the nucleate boiling region, great care was taken to obtain a reproducible surface. After each series of runs the first run of the series was repeated to check the surface conditions. No surface changes were noted during the nitrogen runs; however, the Dow Corning 630 electronic protective coating, which was placed on the end plates of the heat transfer element, was attacked by liquid methane and deposited on the heater surface. This fouling necessitated removing the heat transfer element from the pressure vessel and cleaning it with methanol and acetone. The nitrogen run at a pressure of 389 pounds per square inch was then repeated to see if the surface had been restored to its original state, and it checked.

The heat transfer surface was kept in a nitrogen or a methane atmosphere between runs to insure that no contaminating gas was adsorbed on the heater surface.

The heat transfer element was allowed to return to room temperature several times during the investigation; this cycling apparently did not affect the surface condition of

the heater. Lyon (37) obtained similar results in his study of boiling heat transfer to nitrogen and oxygen.

Since hysterisis effects have been noted in nucleate boiling (12,34), particular care was taken to always increase the heat flux while nucleate boiling data were being obtained. Run 9 which was briefly interrupted by a power failure and was started again at the same flux yielded flux values which were high.

Several investigators (12,26,34) have reported a variation of the heat transfer coefficient with time for a newly immersed heat transfer surface. This effect was noted in this investigation; however, after 30 minutes the surface had reached a steady state and no variation was found at longer times. Because of this time dependence, the liquid was allowed to boil at least 30 minutes at the start of each series of runs before data were taken. After the heat transfer surface had been in the film boiling region, it took only a few minutes to reach a steady state condition after it was returned to the nucleate boiling region.

At the start of each series of runs the system was cooled by charging liquid nitrogen into the system and venting the vapor to the atmosphere. For nitrogen runs the vent and fill line were closed when the liquid level in the autoclave was approximately 6 inches. For methane runs, the nitrogen used for precooling was allowed to vaporize; then the methane was charged until the depth of the liquid was approximately 6 inches. During the methane charging, the

vent line was left open so small amounts of methane could vaporize into the atmosphere and purge any nitrogen which was left in the system. The liquid nitrogen coolant was circulated through the condensing coil during the cooling and filling operations to cool the system faster. After the pressure vessel was filled, the pressure required was obtained by adjusting the metering valve which controlled the nitrogen coolant stream. The heat transfer element was then turned on and the temperatures, amperage, and voltage values were recorded after equilibrium was reached. After each increase in power the pressure was adjusted, and a new set of readings was obtained.

The experimental values in the film boiling region took considerable time to obtain because of the time required for the heat transfer element to reach equilibrium. The added resistance to heat flow caused the tungsten winding to heat up which changed its resistance. It was found that the time required for the heat transfer element to reach equilibrium in the film boiling region could be shortened by setting the voltage slightly above the value wanted and then decreasing the voltage to the value which was to be recorded. This procedure was also effective for the region above the critical point.

During the investigation, the teflon sealant in the Conax fittings cold flowed. This flow necessitated tightening these fittings every 2 hours to prevent leakage.

Since the cooling capacity of the system was not

great enough to obtain the entire nucleate boiling curve for methane, film boiling was initiated by raising the pressure above the critical pressure then reducing it to the pressure which was of interest.

The atmospheric nitrogen data were obtained by immersing the heat transfer element in a 5 liter dewar of liquid nitrogen. Make-up nitrogen was added when the liquid level reached a point 6 inches above the heat transfer surface.

To insure that no air would be drawn into the system due to a vacuum the methane pressure was always held in excess of 10 pounds per square inch gauge.

CHAPTER V

DERIVATION OF EQUATION FOR CRITICAL TEMPERATURE DIFFERENCES

Because of surface effects which cannot be characterized, nucleate boiling critical heat fluxes and the corresponding temperature differences reported by various workers are widely different for a given substance. Since the characterization of the surface effects has not yet been accomplished, a method of comparing nucleate boiling burnout data of various investigators which eliminates surface effects is needed. Such a method would not only allow the data of different investigators to be compared but would also provide a method by which the surface could be characterized.

To date, attempts to correlate burnout data have been primarily concerned with the critical heat flux. Frederking's work is the exception. Since the critical heat flux has received wide attention with little success, this work will be primarily concerned with the critical temperature difference.

The following derivation will be restricted to corresponding states liquids. This restriction will eliminate some of the complications which occur due to the molecular interactions of the more complicated substances.

A logical starting point for any correlation, which

eliminates the effect of surface conditions at the burnout point, is an analysis of the variables which effect ϵ as defined by Frederking (see equation 8-a). ϵ will certainly depend on the geometry of the heat transfer element and the number of potential nucleation sites. Since the number of nucleation sites for a given surface which are active depends upon the level of superheat (11,28,34), it seems reasonable to assume that ϵ will depend upon the thermodynamics of the liquid being boiled. It will therefore be assumed that ϵ can be specified by an equation of the form given below

$$\epsilon = f'(\varphi, N, T_r) \qquad (13)$$

Where: φ is a geometric shape factor.

N is the number of potential nucleation sites for a given surface.

If the equation above is valid, ϵ should be equal for liquids, which follow the law of corresponding states, that are boiled on the same heat transfer surface. A plot of Lyon's data (37) for oxygen and nitrogen boiling on a platinum surface (Figure 5) shows that ϵ is not dependent on the liquid being boiled up to a reduced temperature of 0.85. Unfortunately Lyon's heat transfer element was partially in the film boiling region at high pressures so values of ϵ above a reduced temperature of 0.85 for oxygen could not be calculated. However, the close correspondence at pressures below 15.51 atmospheres tends to prove the validity of assuming equation 13.

The effect of surface effect and the effect of the

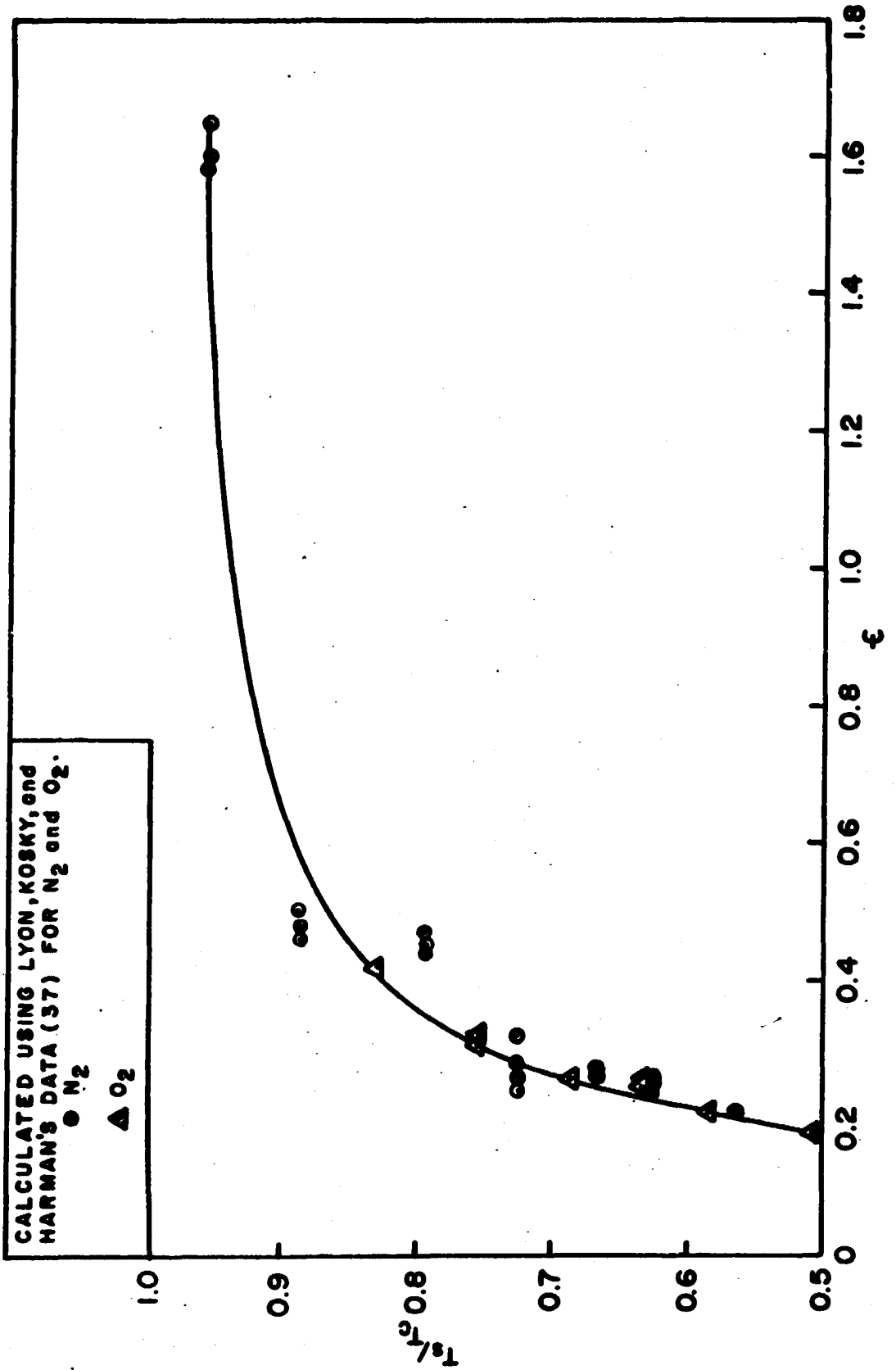

Figure 5. Variation of ε With Reduced Temperature

surface geometry can be eliminated by setting a reference value of ϵ on each surface and dividing all the ϵ's by this reference value; that is, ϵ at a given reduced pressure will be assumed as a reference value. This procedure yields:

$$\frac{\epsilon}{\epsilon_{ref}} = \frac{\Delta T_{bo}}{\Delta T_{vw}} \times \frac{\Delta T_{vw\ ref}}{\Delta T_{bo\ ref}} = \frac{f'(\varphi, N, T_r)}{f'(\varphi, N, T_{r\ ref})}$$

Since the geometric factor and the number of potential active nuclei will be constant for a given surface, the above equation reduces to:

$$\left[\frac{\Delta T_{bo}}{\Delta T_{bo\ ref}}\right]_{N\varphi} = \frac{[f'(T_r)]_{N\varphi}}{[f'(T_{r\ ref})]_{N\varphi}} \left(\frac{\Delta T_{vw}}{\Delta T_{vw\ ref}}\right)$$

$$= \frac{[f'(T_r)]_{N\varphi}}{[f'(T_{r\ ref})]_{N\varphi}} \cdot \frac{f''(T_r)}{f''(T_{r\ ref})}$$

or since $[f'(T_{r\ ref})]_{N\varphi}$ and $f''(T_{r\ ref})$ represent constants then,

$$\frac{\Delta T_{bo}}{\Delta T_{bo\ ref}} = f(T_r) \qquad (14)$$

Equation 14 should be valid for pool boiling of liquids which follow the law of corresponding states to a high degree of accuracy. The geometry of the heat transfer element should not be a factor with the possible exception of thin wires, where the bubble diameter approaches the diameter of the wire. The equation will probably also hold for a series of substances that are thermodynamically similar.

CHAPTER VI

RESULTS AND DISCUSSION

The usual manner of representing boiling heat transfer is to present a plot of the logarithm of the temperature difference versus the logarithm of the heat flux. This procedure tends to mask the scatter of the data and can be deceiving to the cursory observer. For this reason, all data obtained in this investigation will be presented as plots of the temperature difference versus the heat flux. Since the heat fluxes and temperature differences obtained with cryogenic liquids are lower than those obtained with higher boiling liquids, the additional range afforded by log-log plots is not required for presentation of the data.

The discussion of the experimental results will be divided into four areas: nucleate boiling below the critical heat flux, the critical heat flux, film boiling, and convective heat transfer at pressures which exceed the liquid's critical pressure.

While operating in the nucleate boiling region a temperature gradient around the circumference of the element was noted. Similar gradients have also been noted by previous

investigators (16,26). The values for the temperature differences 60° from the top (measured from the vertical axis) and at the bottom of the element for a representative run are plotted versus the heat flux in figure 6. The variation in temperature around the circumference is less than 2°F. This behavior was noted on all nucleate boiling data and seems to be independent of pressure level. The variations in temperature around the circumference which were found in this investigation were larger than those reported by Haselden (26). He used a 3/8 inch diameter heat transfer element as compared with a diameter of 0.8022 inches used in this investigation, suggesting that the variations in temperature with circumference increase with increasing diameter of the heat transfer element. This variation around the circumference poses the problem of what temperature difference should be used. The temperature difference obtained from the thermocouples located 60 degrees from the top were chosen as representative in this investigation since there were two thermocouples at this angular location which provided a check on the temperature difference.

During the investigation, several runs were repeated to check whether the surface had undergone a change. It was found that for a given heat flux the temperature difference could be reproduced within 10 per cent. The 4 nitrogen runs conducted at atmospheric pressure are plotted in Figure 7 to give the reader a feeling for the reproducibility of the data.

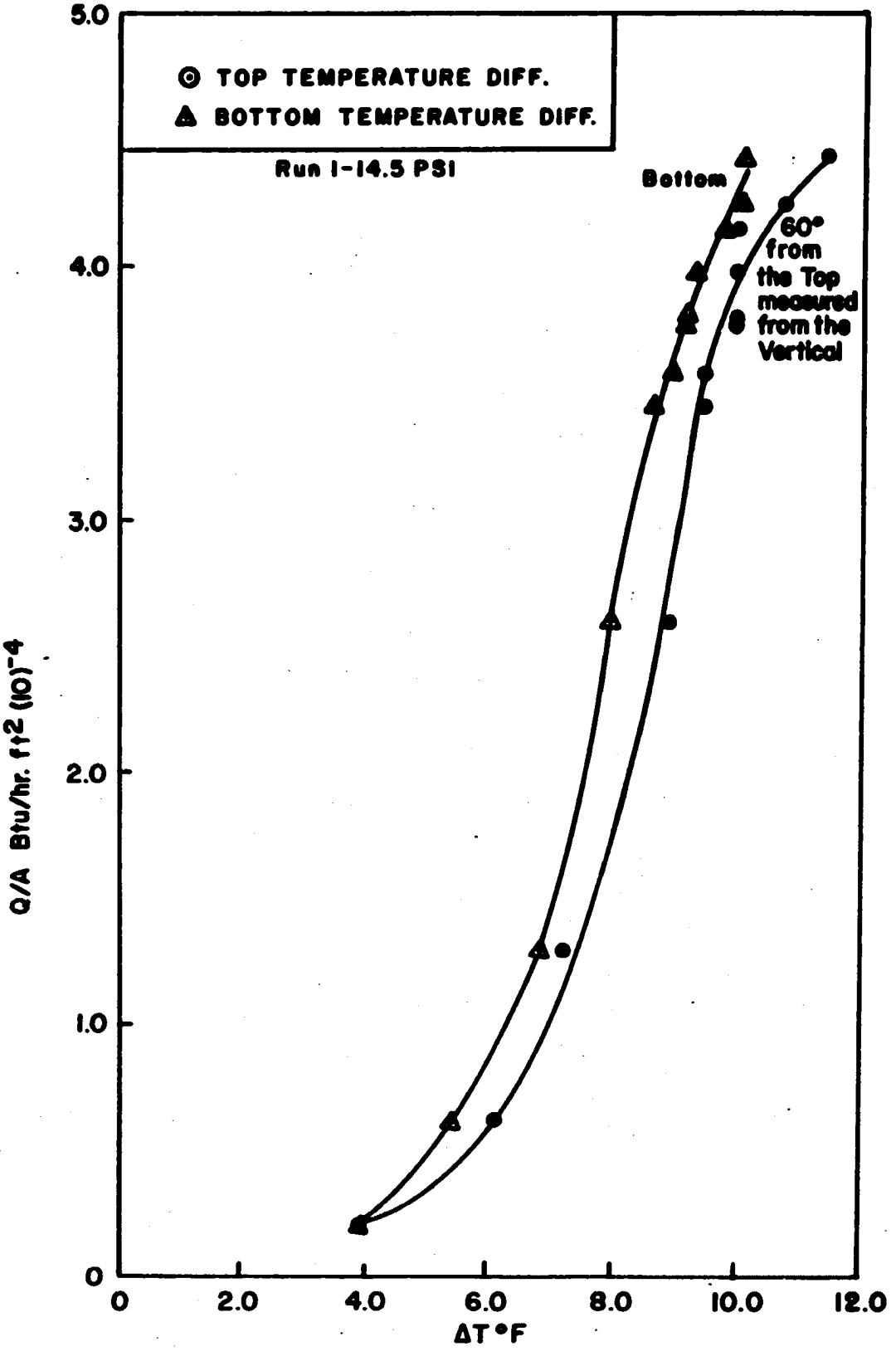

Figure 6. Comparison of ΔT at the Top of the Heat Transfer Element With ΔT at the Bottom of the Element

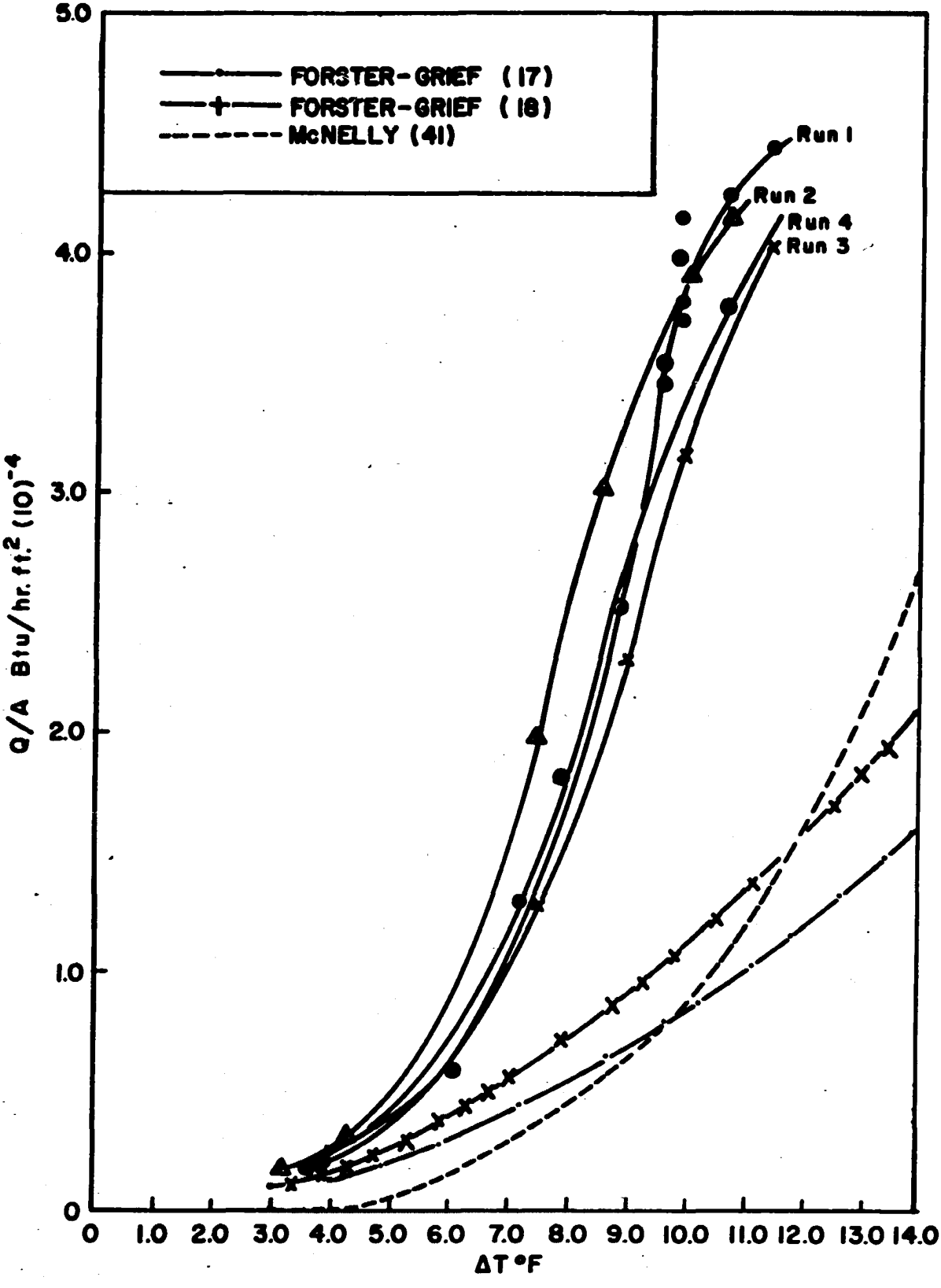

Figure 7. Nucleate Boiling ΔT Vs Heat Flux For N_2 at 14.5 psia Compared With Correlating Equations

Figure 7 also includes 3 nucleate boiling correlations which are commonly used to predict nucleate boiling design data. It is obvious that these correlations deviate from the experimental data enough to be of little value other than for rough approximations. The higher pressure data were not compared with the correlating equations since it was apparent that the equations give heat fluxes which are low for a given temperature difference. To predict nucleate boiling data a correlation must account for surface conditions. As yet, not enough is known about the surface contribution to allow such a correlation to be formulated.

An increase in the temperature difference with time, when the heat transfer element was first immersed in liquid nitrogen, was noted; however, after thirty minutes the temperature difference had reached a constant value and the data were reproducible. A time effect was also noted when the heat transfer element had been in the film boiling region prior to the nucleate boiling run. The time effect was not as pronounced when the element had been in film boiling. The temperature differences under these conditions became constant after two or three minutes. Exposing the heat transfer element to room conditions had an effect similar to that found when the element had been in film boiling.

The effect of pressure on nucleate boiling nitrogen and methane is shown in Figures 8 and 9. The nucleate

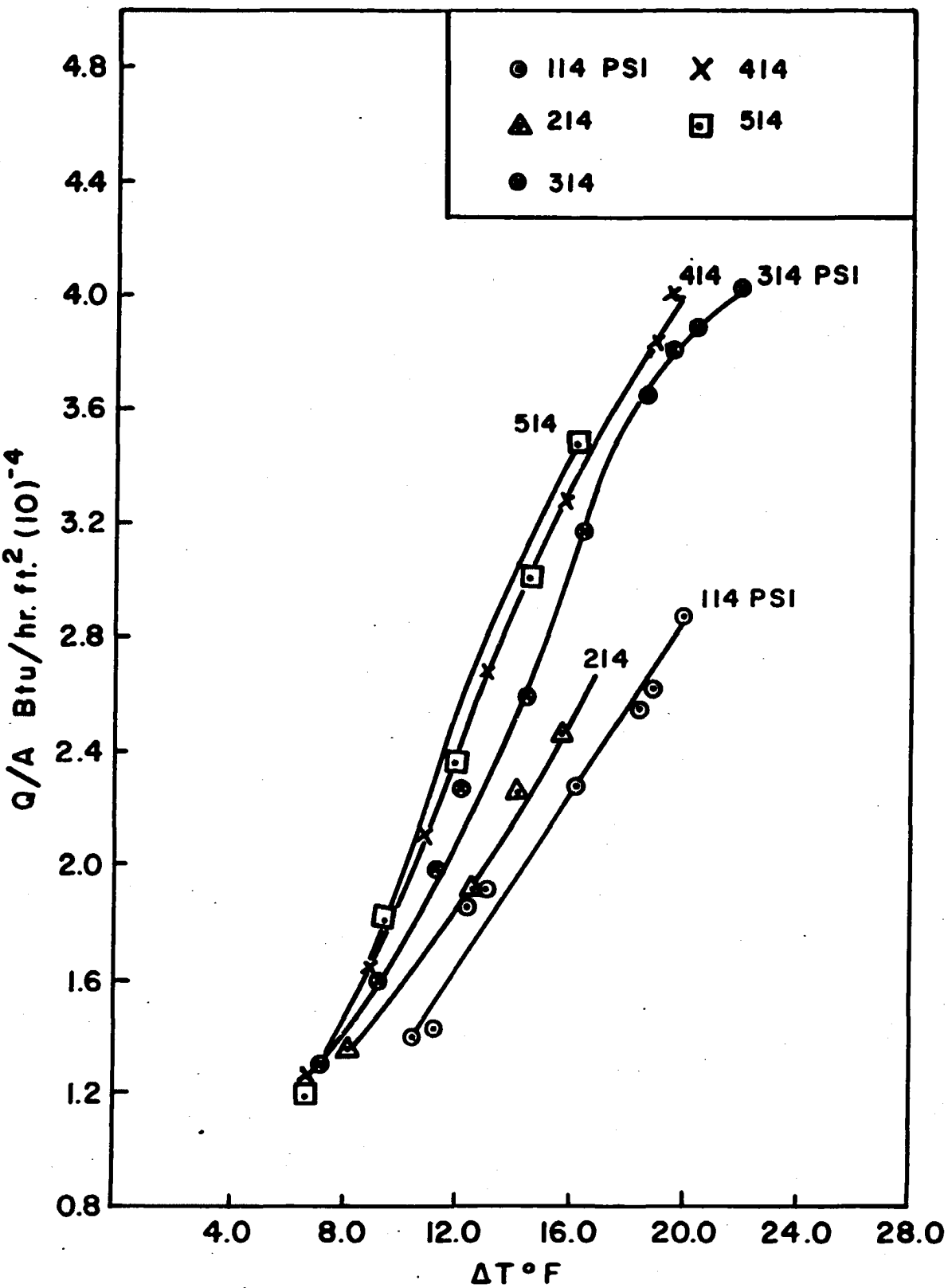

Figure 8. ΔT Vs Heat Flux For Methane Nucleate Boiling

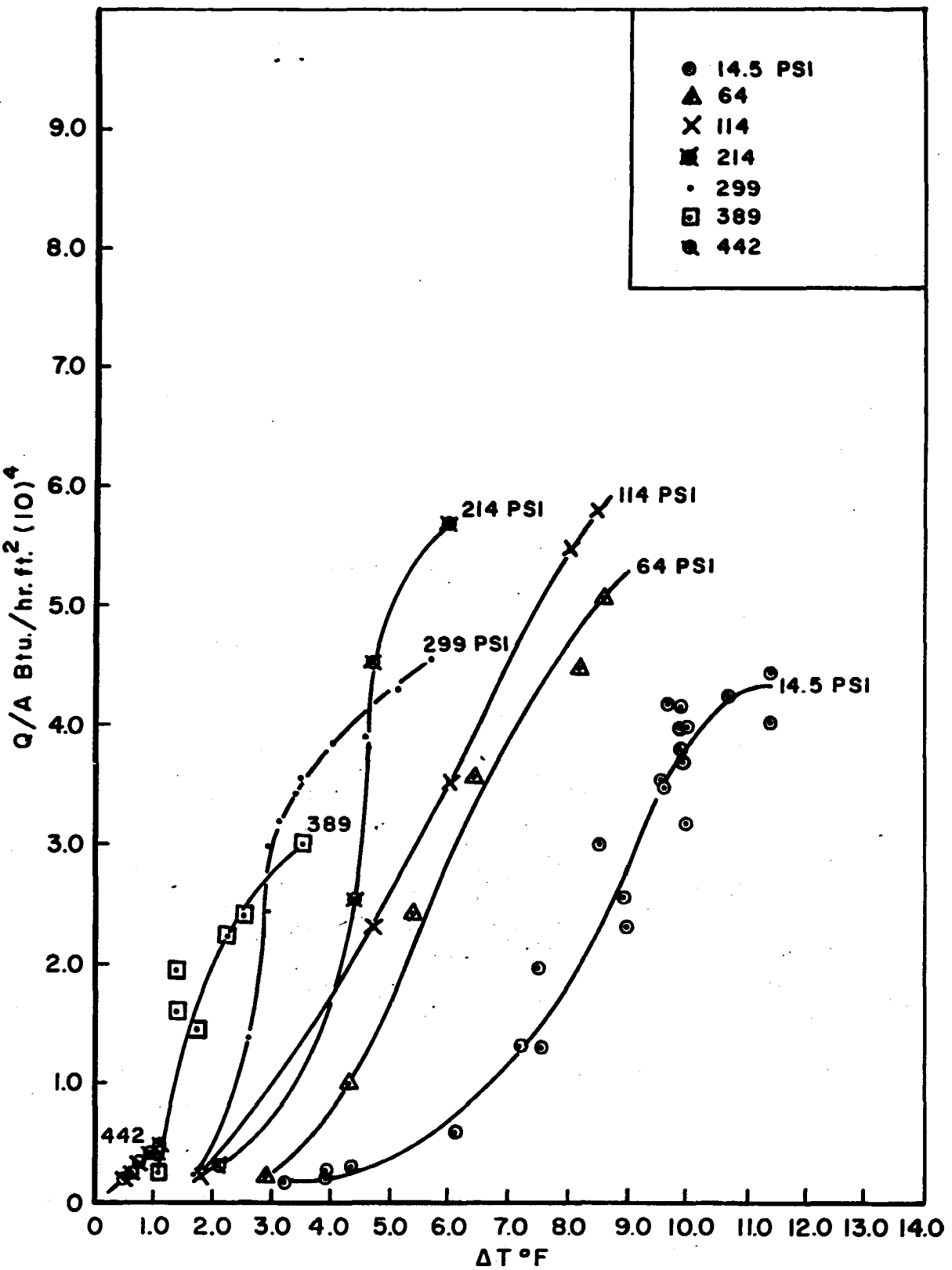

Figure 9. ΔT Vs Heat Flux For Nitrogen Nucleate Boiling

boiling curves for nitrogen and methane shift to the left with increasing pressure as expected. However the nitrogen curves for 299 and 389 pounds per square inch reach temperature differences which are higher than the ones at lower pressures for a given heat flux. This effect occurs as the critical heat flux is approached. Lyon (37) reports this type of behavior for nitrogen boiling on a platinum plate. Roubeau (50), however, does not report this behavior for nitrogen boiling on a copper plate. He does report a leveling out of the curve as the burnout point is approached. This previous work coupled with the fact that the run at 389 pounds per square inch was reproduced tends to confirm that this effect is indeed present, at least for boiling nitrogen on gold and platinum surfaces.

Preliminary runs at atmospheric pressure for nitrogen on a copper surface shifted the nucleate boiling curve to the right. Fouling of the surface was found to shift the nucleate boiling curves to the left.

Due to inadequate cooling for condensation of methane at high heat fluxes, the critical heat flux for methane was not obtainable with the equipment used in this investigation. Therefore, the discussion of the critical heat flux and critical temperature difference is restricted to data obtained with the nitrogen system. The critical heat flux at

a given pressure level varied less than 9 per cent when runs were repeated to check surface conditions.

The critical temperature differences were found by extrapolating the temperature difference to the burnout point as suggested by Cichelli and Bonilla (10). The extrapolated values of the critical temperature difference for a given pressure level were within 10 per cent of each other in all cases.

The variation of the critical heat flux with reduced pressure is shown in Figure 10. The experimental data of Lyon, Kosky, and Harman (37) for the critical heat flux of nitrogen boiling on a platinum plate and Roubeau's (50) recommended curve for nitrogen boiling on a copper plate are also presented for comparison purposes. It is apparent from Figure 10 that the surface, or a combination of the surface and heat transfer element geometry, has a significant effect upon the critical heat flux. (A similar conclusion was advanced by Gambill (23)).

In Figure 11 several of the common critical heat flux correlations which neglect surface and heat transfer element geometry are compared with the experimental data obtained in this investigation. Figures 10 and 11 show no single equation plotted can predict the results of Roubeau (50), Lyon et al., and this investigation.

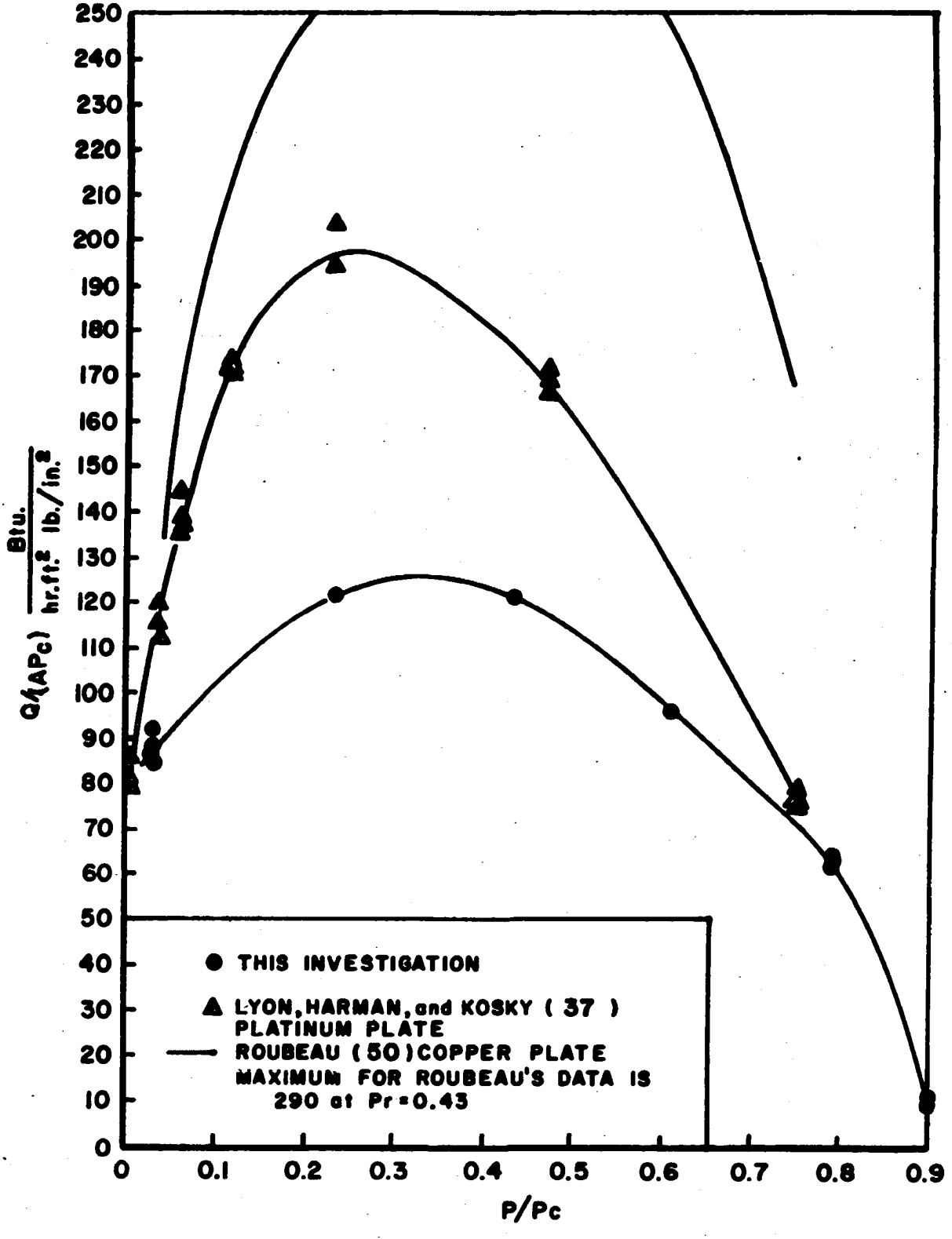

Figure 10. Comparison of the Critical Heat Flux Data With Previous Data

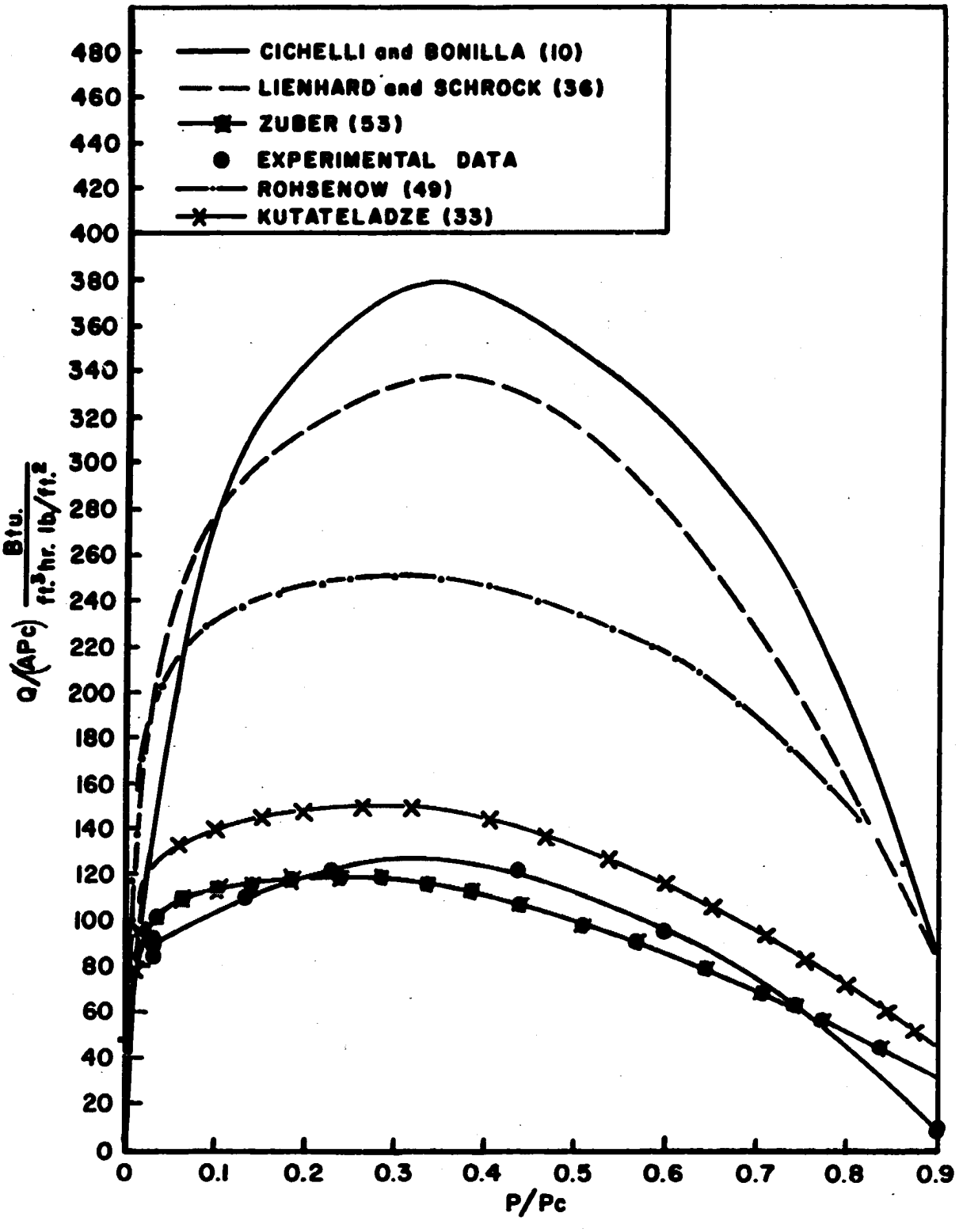

Figure 11. Comparison of the Critical Heat Flux With Predicted Values For Nitrogen

The critical temperature difference values obtained in this investigation are compared with Frederking's proposed equation (19,20) in Figure 12. The poor agreement of the data with the equation is to be expected. As was pointed out by Frederking, the proposed relationship is a rough approximation and cannot be used for quantitative predictions.

A comparison of the values of ϵ obtained in this work with those of Lyon is given in Figure 13. The difference in ϵ at any given temperature can be attributed to the fact that Lyon used a flat platinum plate whereas in this investigation a gold plated cylinder was used.

The validity of equation (14) derived earlier in this work, was checked by plotting Lyon, Kosky and Harman's nitrogen and oxygen data; Roubeau's nitrogen data; and the data obtained in this investigation (Figure 14). The curve drawn through the data is a least squares fit for an equation of the following type.

$$\frac{\Delta T_{bo}}{\Delta T_{bo} \text{ at } P_r=0.1} = a(1 - T_r)^n \qquad (15)$$

The values of a and n respectively were found to be 2.3 and 0.64. Of the 71 data points available for the least squares

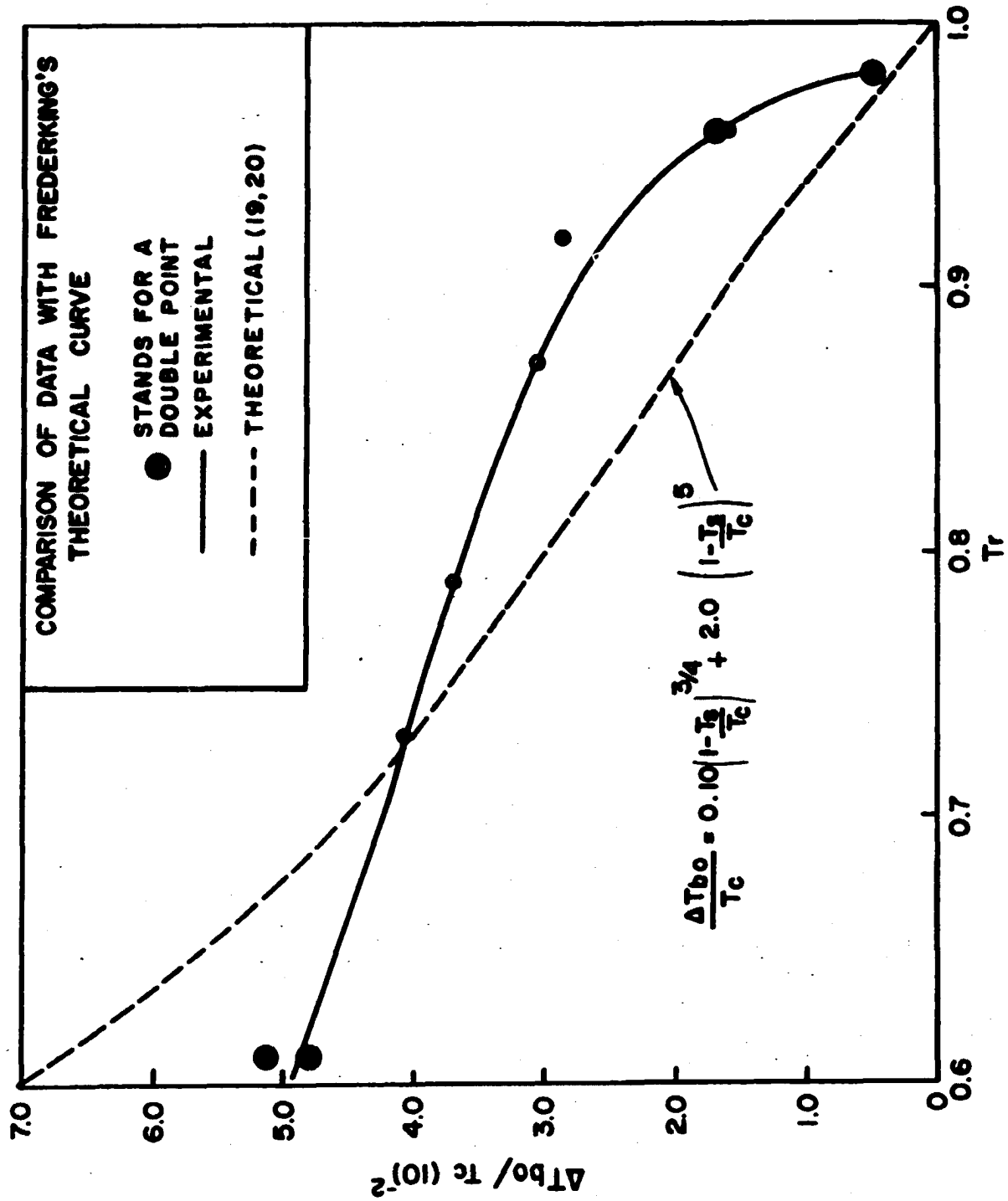

Figure 12. Comparison of the Data For Critical Temperature Differences With Frederking's Predicted Curve

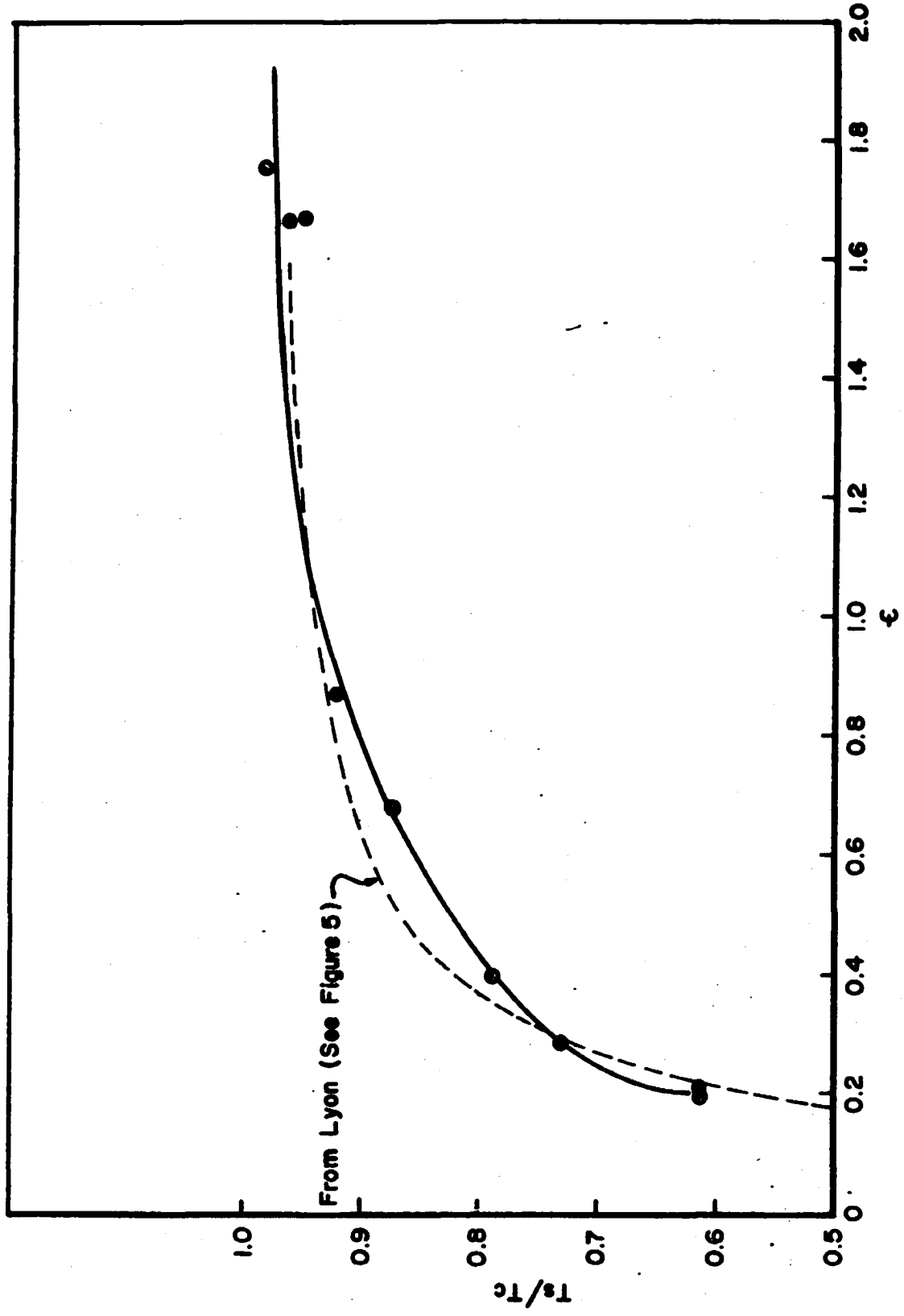

Figure 13. Variation of ε With Reduced Temperature For This Investigation

fit, 86 per cent of them deviate from equation 15 less than 15 per cent and 97 per cent of them deviate from the equation less than 30 per cent. In view of the scatter (10 per cent in this investigation) which seems to be inherent in boiling heat transfer data, it is felt that the correlation predicts the data remarkably well. Equation 15 is expected to be valid for any liquid which follows the law of corresponding states to a high degree of accuracy; however, experimental data for all substances which meet this requirement are necessary before generality can be claimed. Equation 15 was compared with data on substances which do not follow the law of corresponding states by plotting Addom's data on water (40) and Cichelli and Bonilla's data for organic liquids (10) (see Figure 15). The equation fits this data well for values above a reduced temperature of 0.7, but wide deviations are noted at lower saturation temperatures. The reader is cautioned against using equation 15 for predicting temperature differences at high pressures from low pressure data for substances which do not follow the law of corresponding states to a high degree of accuracy. Equation 15 was derived for corresponding states liquids and should be restricted to those liquids until sufficient data are available to test the equation for substances which do not follow the law of corresponding

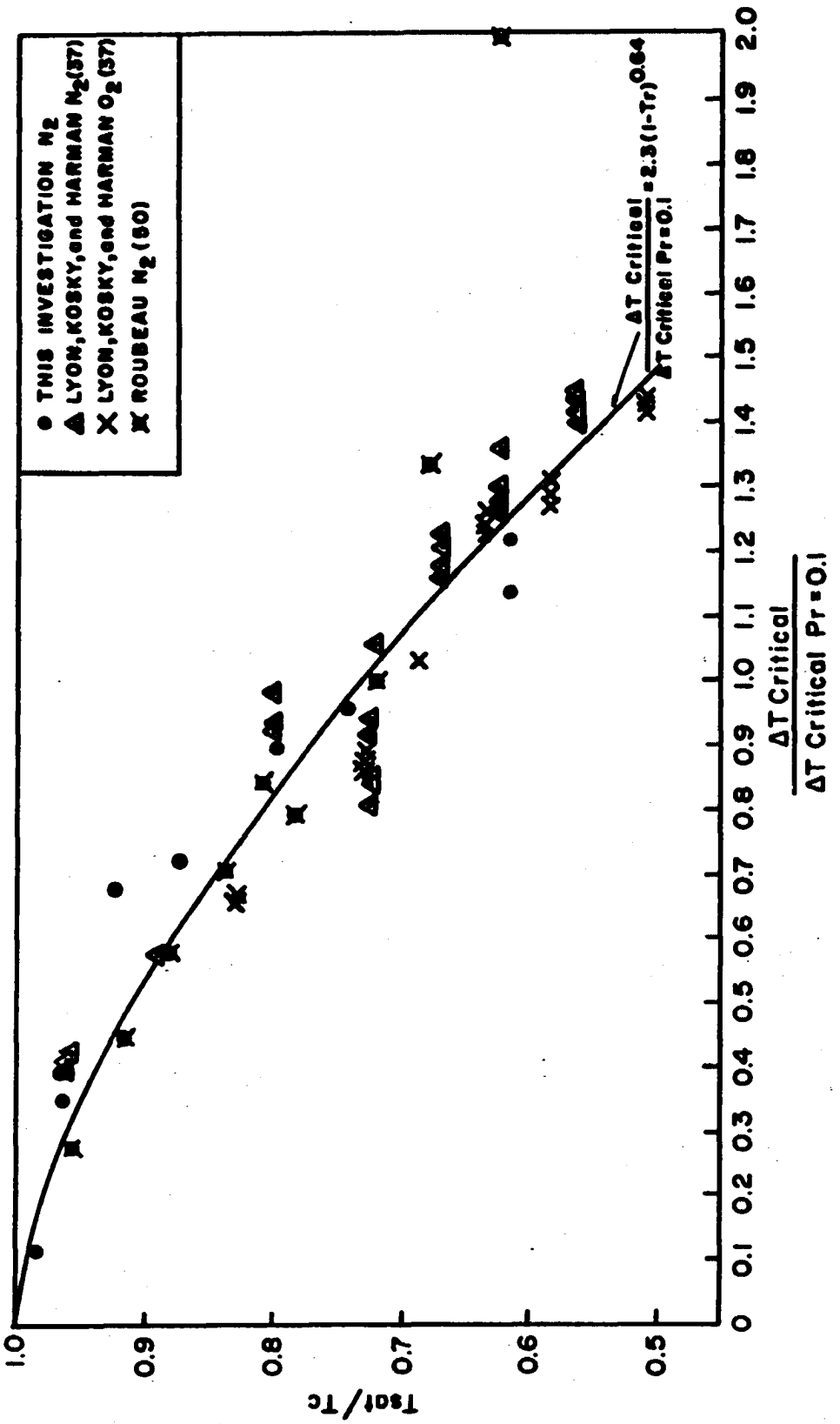

Figure 14. Comparison of Available Data With Equation 15

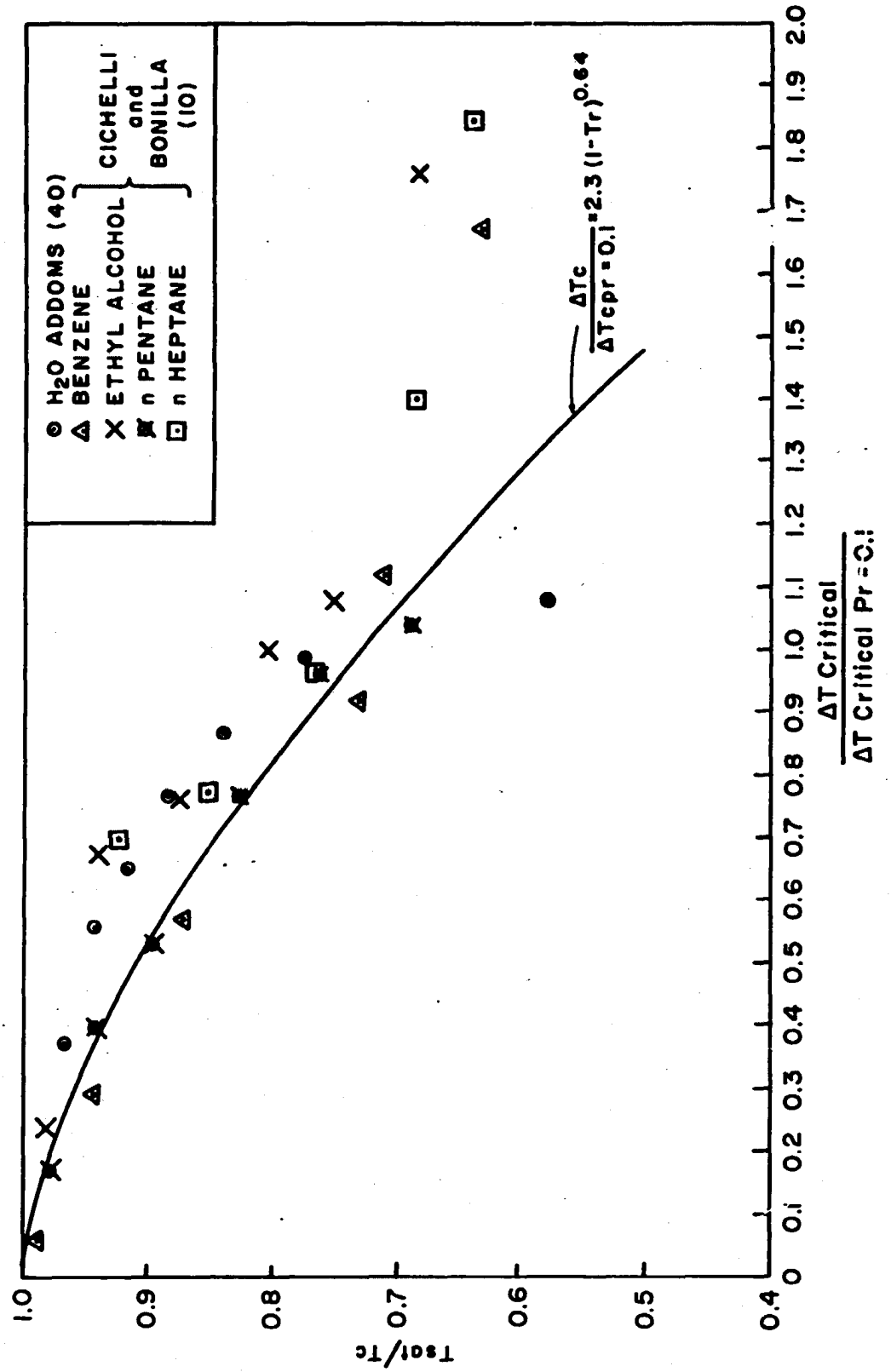

Figure 15. Comparison of Data For Liquids Which Do Not Follow the Law of Corresponding States With Equation 15

states.

The experimental data for nitrogen and methane stable film boiling at various pressure levels are presented in Figures 16 and 17. Banchero, Barker and Boll's (1) data for film boiling oxygen at several pressure levels are plotted in Figure 18 for comparison purposes. It is believed that these 3 sets of data are the only ones which have been reported over a pressure range. The curves for pressures of 442 pounds per square inch for nitrogen and 614 pounds per square inch for methane from this present study clearly show that the heat flux at a given temperature decreases rapidly as the critical pressure is approached. This effect is not apparent in Banchero's work; however, his highest pressure run corresponds to a reduced pressure of 0.66 while this effect is noted in the present study at reduced pressures of 0.91 for methane and 0.9 for nitrogen. Therefore, a rapid decrease in heat flux as the critical pressure is approached would not be noticeable in Banchero's data. The effect of pressure on the runs which are at a reduced pressure lower than 0.8 appears to depend upon the magnitude of the temperature difference. For high temperature differences an increase in pressure increases the heat flux for a given temperature difference. For low temperature differences an increase in pressure will decrease the heat flux for a given temperature

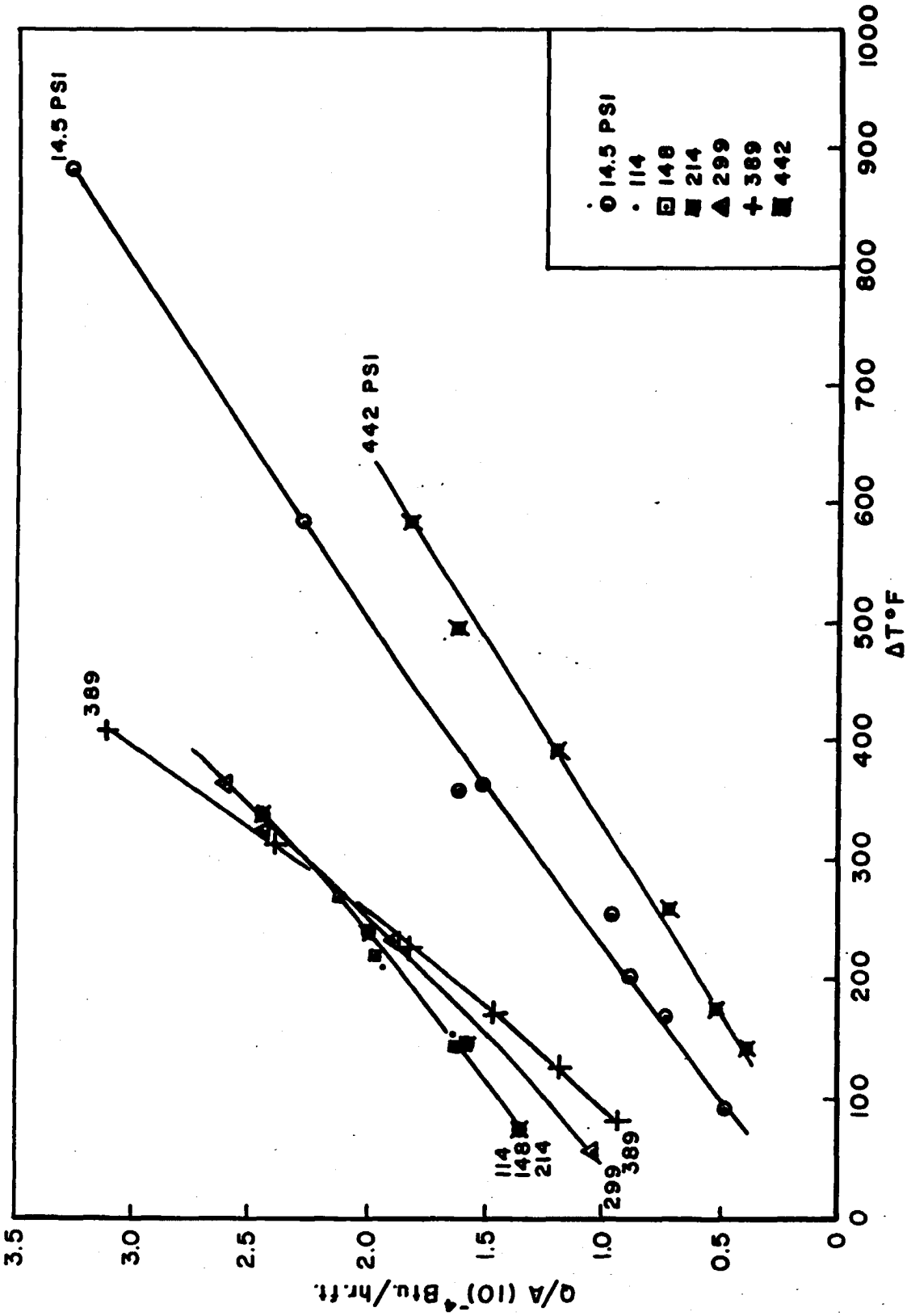

Figure 16. ΔT Vs Heat Flux For Nitrogen Film Boiling

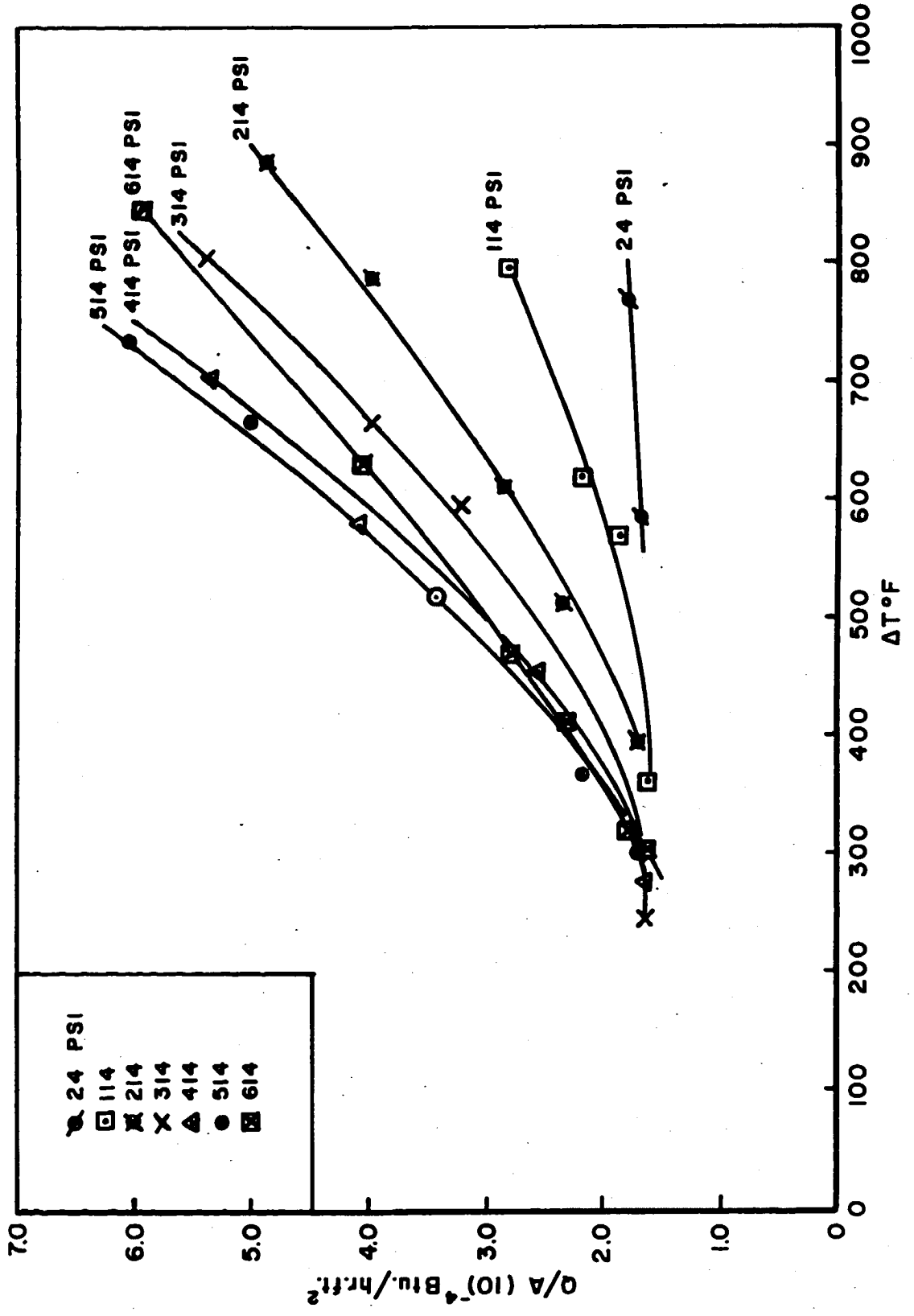

Figure 17. ΔT Vs Heat Flux For Methane Film Boiling

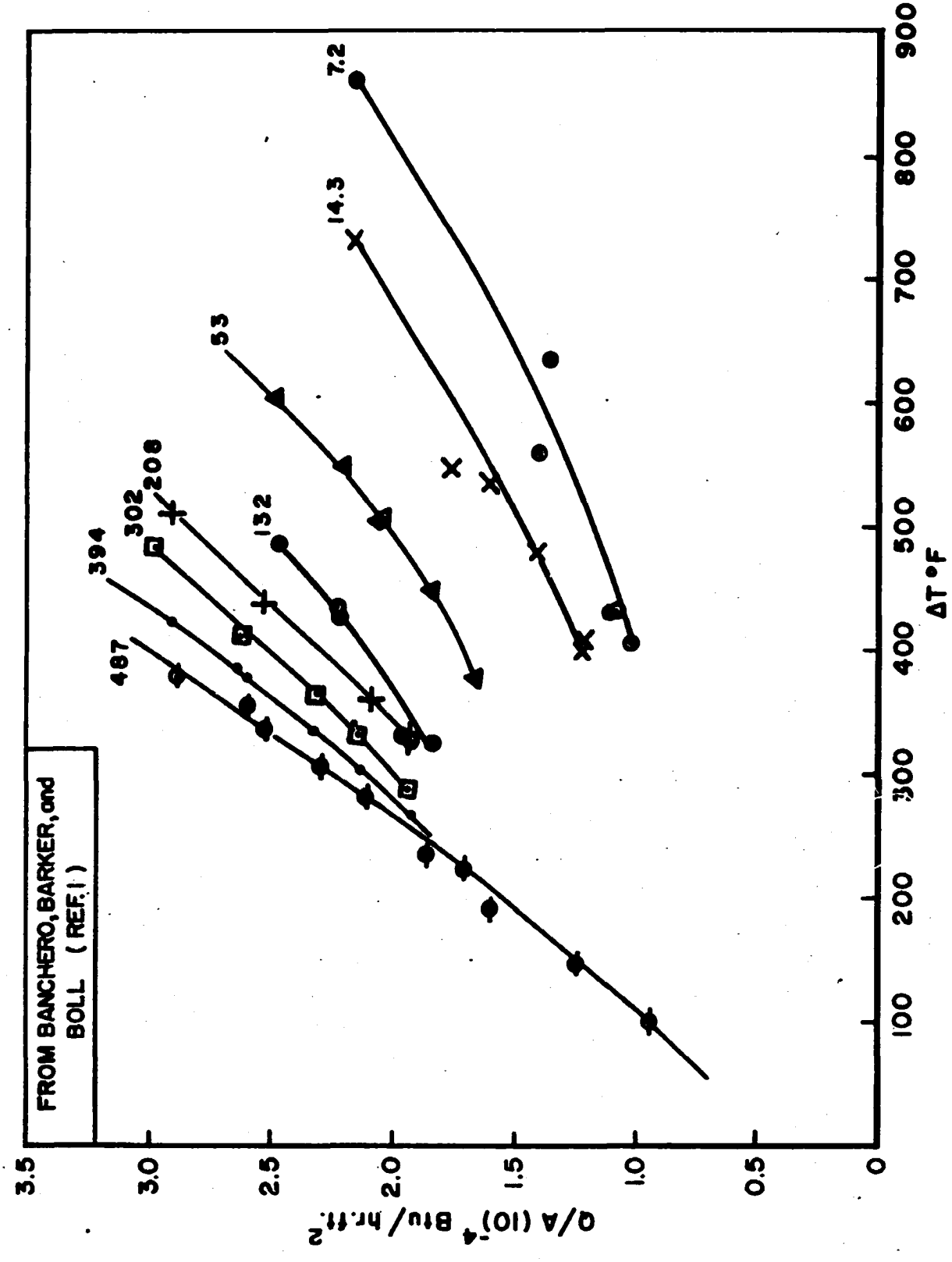

Figure 18. ΔT Vs Heat Flux For Oxygen Film Boiling

difference. The behavior of the nitrogen curve at a pressure of 14.5 pounds per square inch leads to the conclusion that at low pressures this transition behavior probably does not occur. There is insufficient data available, however, to predict the pressure below which the film boiling curves will not cross. The temperature differences above which the heat flux will increase with increasing pressure appear to be approximately 350°F for nitrogen, 400°F for methane, and 350°F for oxygen.

The experimental data for film boiling methane and nitrogen are compared with Breen and Westwater's predicted curve (equation 12) in Figures 19 and 20. The only restriction placed on the predicted curve was that the diameter of the heat transfer element did not equal (6) "the most dangerous wave length" (i.e., the wave length whose amplitude increases at the fastest rate). The diameter of the heat transfer element used in this investigation was 0.06685 feet. "The most dangerous wave length" varied from 0.0104 feet at 614 pounds per square inch to 0.063 feet at 24 pounds per square inch for methane and from 0.0065 feet at 442 pounds per square inch to 0.04 feet at 14.5 pounds per square inch for nitrogen. Therefore these data provide a test of the generality of Breen and Westwater's equation. Figures 19 and 20 clearly show that the equation is not general. The factor,

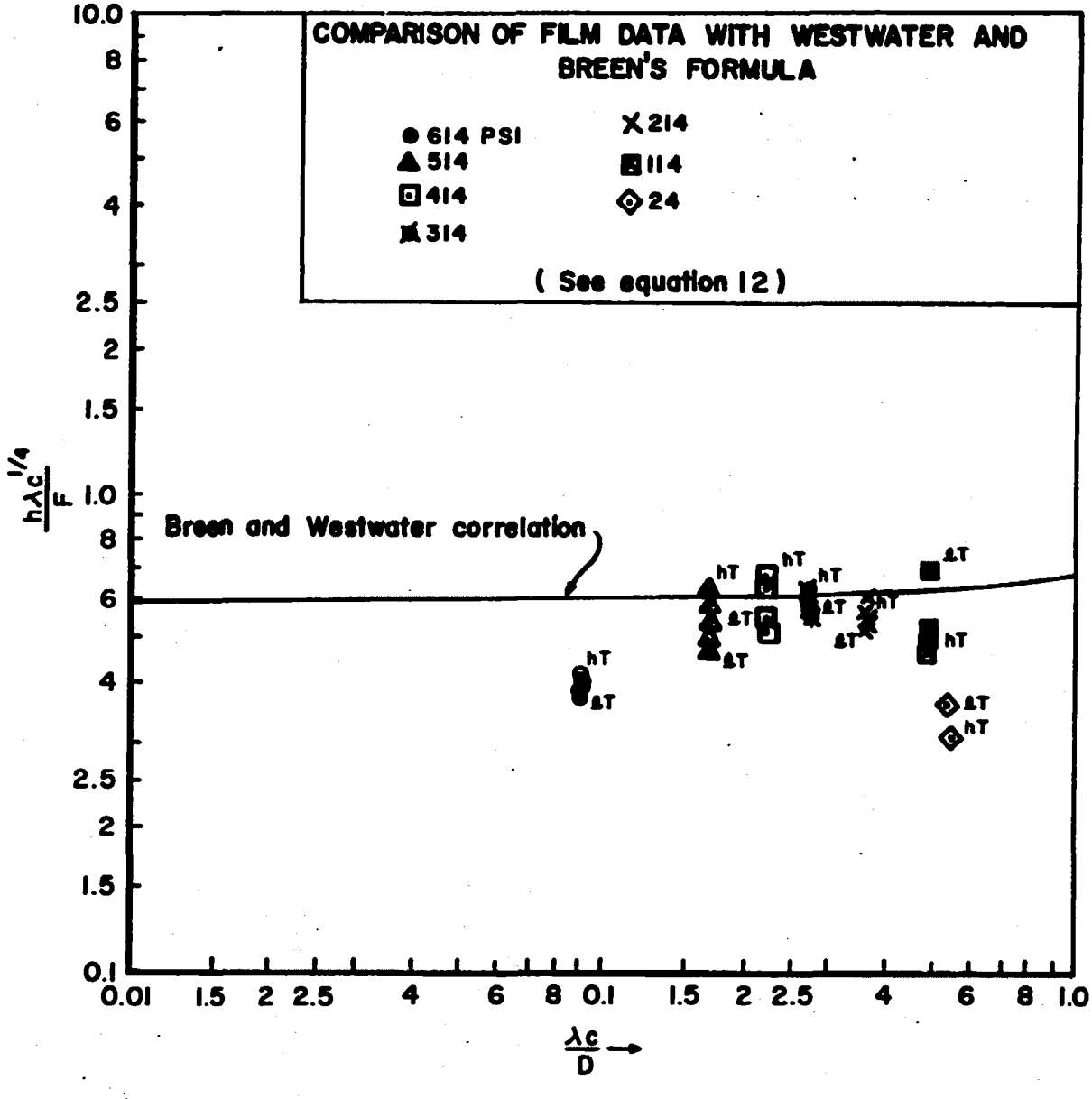

Figure 19. Comparison of Methane Film Boiling Data With Equation 12

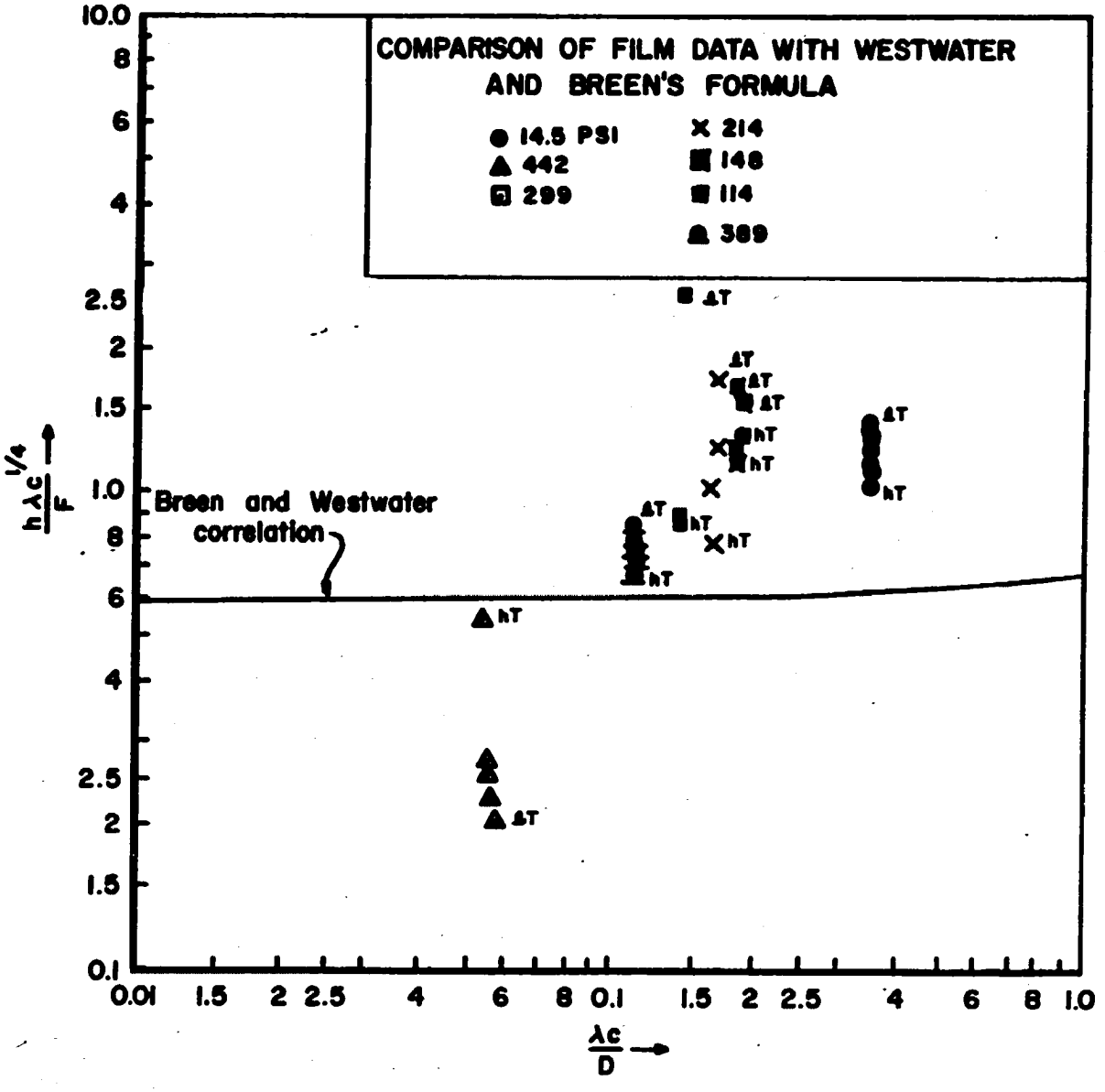

Figure 20. Comparison of Nitrogen Film Boiling Data With Equation 12

$\frac{h\lambda_c^{1/4}}{F}$, is dependent upon the temperature difference which also casts doubts on the equation's generality. It is interesting to note that the highest temperature difference (hT in Figures 19 and 20) for a given pressure is nearly always the point closest to the predicted curve, while the low temperature difference (ℓT) is almost always the point which shows the most deviation from the curve.

In addition to the boiling heat transfer data which were the primary concern of this investigation, data on convective heat transfer to nitrogen and methane at pressures in excess of their critical pressure were obtained. These data are shown in Figures 21 and 22.

It was found that the heat flux at a given temperature difference was independent of the pressure level for methane in the range of 764 pounds per square inch to 864 pounds per square inch and for nitrogen in the range of 514 pounds per square inch to 814 pounds per square inch. As seen in Figures 21 and 22, if the data at pressures only slightly removed from the critical pressure (492 pounds per square inch for nitrogen; 714 pounds per square inch for methane) are ignored, a straight line will fit the data with an accuracy of 10 per cent.

It was noted that at a specific temperature difference heat transfer in the film boiling region is less

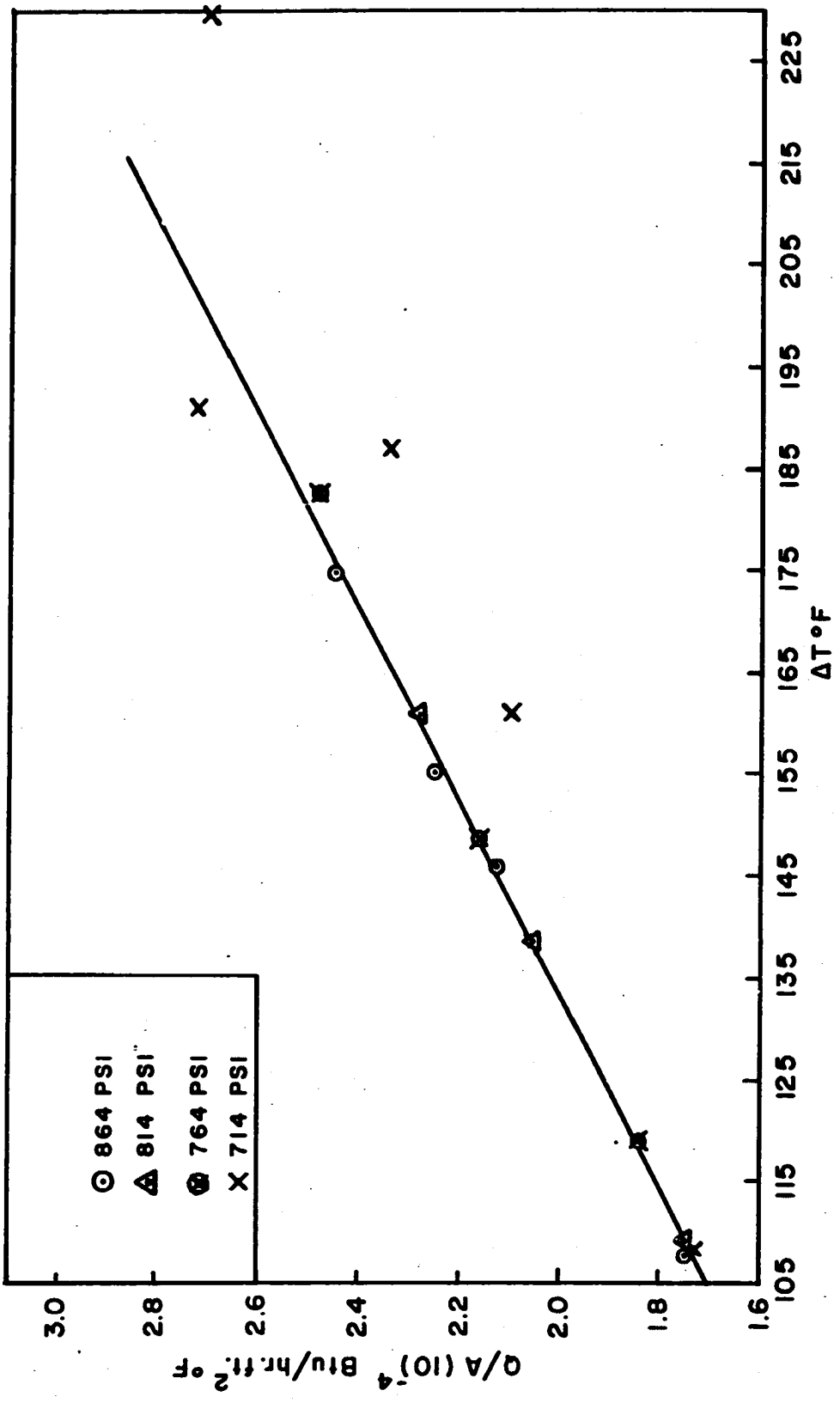

Figure 21. ΔT Vs Heat Flux For Convective Heat Transfer Methane

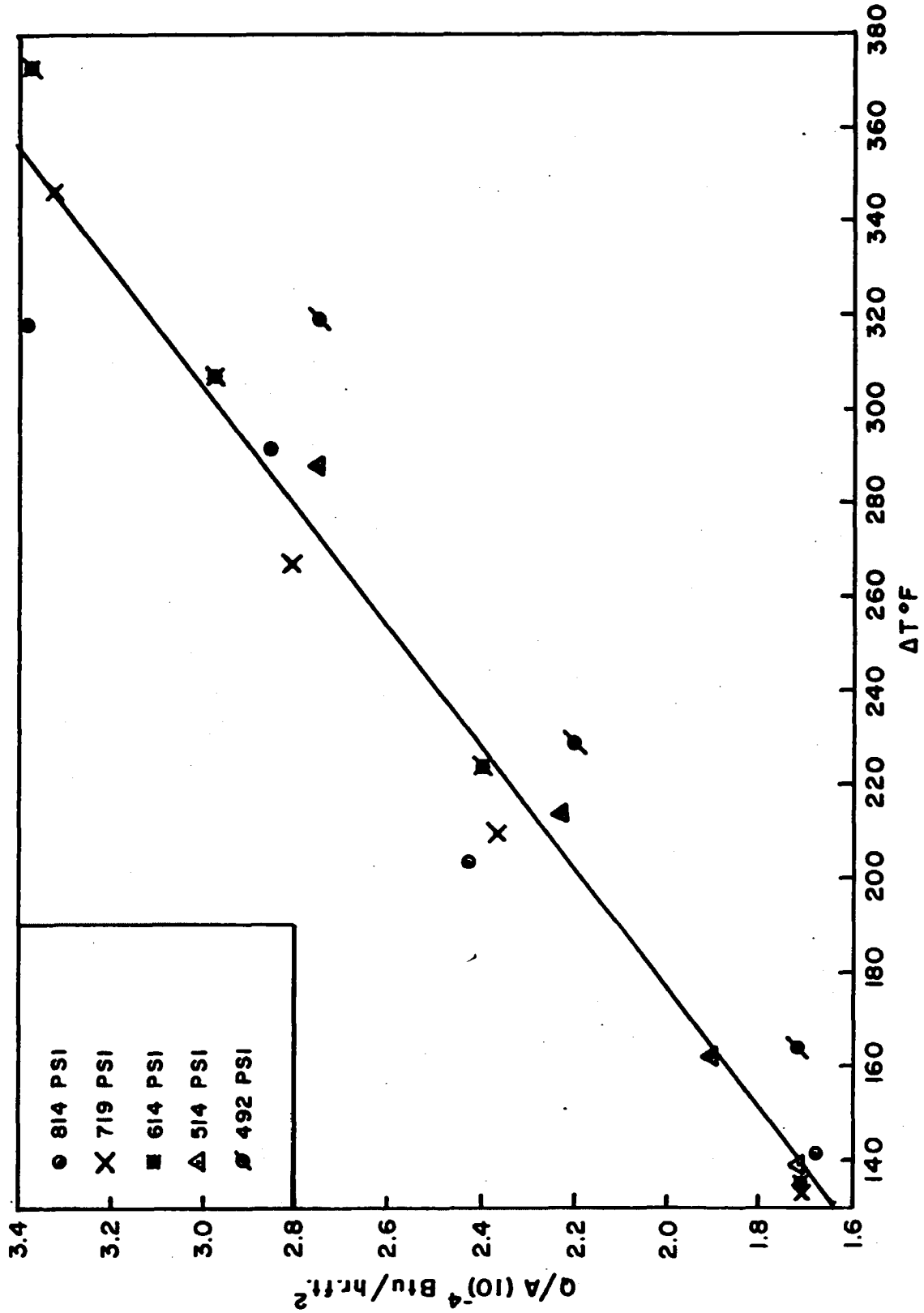

Figure 22. ΔT Vs Heat Flux For Convective Heat Transfer Nitrogen

efficient than heat transfer in the convective region above the critical pressure.

CHAPTER VII

DISCUSSION OF ERRORS

There are two types of errors which are important in boiling heat transfer studies, the errors due to physical equipment or operational limitations and the inherent errors which invariably appear in boiling heat transfer work. The inherent error appears to be of the order of 10 to 15 per cent for boiling heat transfer (14,54). The magnitude of the experimental errors will be discussed for the heat flux measurements, temperature measurements, and the pressure measurements. Experimental errors can be introduced in the heat flux in several ways, inaccurate readings of voltage and amperage, neglect of end losses from the heater, inaccurate heat transfer areas, and neglect of the resistance of electrical leads. The heat transfer area uncertainty and the neglect of the resistance of electrical leads introduce errors whose magnitude is small compared to the errors introduced by other factors; therefore, they can be safely neglected since the relative error for the process of multiplication and division is the sum of the relative errors of the factors involved. The error introduced by neglecting end effects is approximately 2 per cent for the nucleate boiling

region and less than 5 per cent for the film boiling region (see Appendix C). The voltage could be read accurately to ± 0.5 volts for voltages below 25 volts and ± 2.0 volts for voltages above 25 volts. The amperage could be read accurately to ± 0.25 amperes. Therefore the relative error expected in the heat flux is the sum of the relative errors found in the voltage and amperage readings. The errors introduced are of the order of 12 per cent and 7 per cent for heat fluxes of 2000 and 6500 Btu per hr-ft^2, less than 4 per cent for fluxes greater than 12,000 in the film boiling region, and less than 3 per cent for fluxes greater than 12,000 in the nucleate boiling region. Therefore, the reported heat flux for the nucleate boiling region is expected to vary from the correct value by less than 5 per cent at fluxes exceeding 12,000 which represents the majority of the data. The film boiling heat flux is expected to vary from the correct value less than 9 per cent at fluxes exceeding 12,000.

The thermocouple reading could be read accurately to 0.005 millivolts below voltages of 15 millivolts and to 0.025 millivolts above voltages of 15 millivolts. These values correspond to a temperature of 0.25°F and approximately 1°F respectively. Therefore, temperatures taken in the film boiling region are expected to vary from the correct value less than 1 per cent. Values taken in the nucleate boiling region can be expected to vary from the correct value 25 per cent, 5 per cent, 2.5 per cent and 1 per cent at temperature differences of 1°F, 5°F, 10°F and 25°F respectively.

These differences are variations from the actual behavior at the point of the thermocouple junction and not at the surface. In this investigation the values at the surface were assumed to be equal to the values at the junction because the correction factor for surface temperature was less than the gradient around the tube in nucleate boiling and was less than 1 per cent for the film boiling region. The temperatures used were average values of the 3 readings in the film boiling region since the variation of the 3 readings was random and this procedure would in no case introduce errors greater than 5 per cent. The values of temperature measured by the two thermocouples at the top of the heat transfer element were considered the correct values in the nucleate boiling region. To insure correct values of temperature within the accuracy obtainable with the potentiometer used, the thermocouples were calibrated using a platinum resistance thermometer (see Appendix D).

The pressure could be read accurately to 1 pound per square inch (see Appendix E) which gives accuracies superior to those of the temperature differences and heat fluxes.

CHAPTER VIII

CONCLUSIONS

1. The temperature gradient around the circumference of cylindrical heat transfer elements, which was previously reported (16,26), was noted in this investigation during all nucleate boiling runs. The magnitude of these differences depends upon the diameter of the element and temperature difference. The magnitude of the difference appears to be independent of the pressure level.

2. Any generalized correlation of nucleate boiling and critical heat flux should include the effect of surface and geometry.

3. The critical heat flux depends on surface and geometry.

4. The theoretical equation (equation 14) which was derived fits the available data covering oxygen and nitrogen. The equation is expected to be valid for methane, carbon monoxide, argon, nitrogen, krypton, oxygen, and xenon; however more data are required to prove this contention. The final form of the equation is

$$\frac{\Delta T_{bo}}{\Delta T_{bo \text{ at } P_r=0.1}} = 2.3(1 - T_r)^{0.64}$$

5. The film boiling heat flux at a given temperature difference decreases rapidly as the critical pressure is approached. This decrease becomes apparent for nitrogen and methane at reduced pressures greater than 0.9.

6. Breen and Westwater's (6) equation (equation 12 in this text) is not a general equation for film boiling predictions. Their equation may be valid at high temperature differences, but more data are needed to establish this validity. It also appears that the equation could be improved by eliminating the temperature difference dependence, which is apparent in the value of $\frac{h\lambda_c}{F}^{1/4}$.

NOMENCLATURE

A = Area, ft.^{2}

a = Constant in equation 10

c = Constant in equation 10

C_p = Heat capacity, B.t.u./lb. $^\circ F$

D = Diameter, ft.

E = Potential, volts

$$F = \left[\frac{K_v^3 \rho_v (\rho_L - \rho_v) g L [1 + (0.34 C_{pv} \Delta T)/L]^2}{\mu_v \Delta T} \right]^{1/4}$$

g = Acceleration due to gravity

g_c = Conversion factor in Newton's law of motion

h = Heat transfer coefficient, B.t.u./hr. ft.^{2} $^\circ F$

I = Current, amp.

K = Thermal conductivity, B.t.u./hr. ft. $^\circ F$

L = Latent heat of vaporization, B.t.u./lb.

M = Molecular weight

N = Number of potentially active nucleation sites

P = Pressure, P.S.I.

Q = Rate of heat transfer, B.t.u./hr.

R = Universal gas constant

T = Temperature, $^\circ R$

ΔT = Temperature difference, $(T_{surface} - T_{liquid})$

v = Specific volume, ft.^{3}/lb.

Greek Symbols

σ = Surface tension, lb./ft.

$\lambda_c = 2\pi \left[\frac{g_c \sigma}{g(\rho_L - \rho_v)} \right]^{1/2}$

ψ = Parachor

ϵ = Degree of metastability defined by equation 8a

μ = Viscosity

φ = Geometric factor

ρ = Density, lb./ft.^{3}

Subscripts

c refers to the critical point

v refers to the vapor

L refers to the liquid

r refers to a reduced property (T/T_c, etc.)

vw refers to a substance which behaves as predicted by van der Waal's equation

bo refers to the point where the critical heat flux occurs

max refers to the point where the critical heat flux occurs

1 refers to bottom thermocouple

2 refers to thermocouple 60° from the top measured from vertical

3 refers to thermocouple -60° from the top measured from vertical

LITERATURE CITED

1. Banchero, J. T., Barker, G. E., and Boll, R. H., "Stable Film Boiling of Liquid Oxygen Outside Single Horizontal Tubes and Wires," Heat Transfer, Chemical Engineering Progress, Symposium Series, Vol. 51, No. 17, American Institute of Chemical Engineers, New York, 1955, p. 21.

2. Bankoff, S. G., "Prediction of Surface Temperatures at Incipient Boiling," Heat Transfer, Chemical Engineering Progress, Symposium Series," Vol. 55, American Institute of Chemical Engineers, New York, 1959, p. 87.

3. Bankoff, S. G., "Entrapment of Gas in the Spreading of a Liquid Over a Rough Surface," A. I. Ch. E. J., Vol. 4, 1958, p. 24.

4. Berenson, P. J., "Film Boiling Heat Transfer from a Horizontal Surface," J. Heat Transfer, Vol. 83, 1961, p. 351.

5. Borishansky, V. M., Novikov, I. I., and Kutateladze, S. S., "Use of Thermodynamic Similarity in Generalizing Experimental Data of Heat Transfer," Int. Dev. in Heat Transfer Part III, 1961, p. 475.

6. Breen, B. P. and Westwater, J. W., "Effect of Diameter of Horizontal Tubes on Film Boiling Heat Transfer," Chem. Eng. Prog., Vol. 58, July 1962, p. 67.

7. Bromley, L. A., "Heat Transfer in Stable Film Boiling," Chem. Eng. Prog., Vol. 46, May 1950, p. 221.

8. Chang, Y. P., "A Theoretical Analysis of Heat Transfer in Natural Convection and in Boiling," Trans. A. S. M. E. Vol. 79, 1957, p. 1501.

9. Chang, Y. P., "Wave Theory of Heat Transfer," J. Heat Transfer, Vol. 1, Jan. 1959, p. 1.

10. Cichelli, M. T., and Bonilla, C. F., "Heat Transfer to Liquids Boiling under Pressure," Trans. A. I. Ch. E. Vol. 41, 1945, p. 755.

11. Clark, H. B., Strenge, P. S., Westwater, J. W., "Active Sites for Nucleate Boiling," Heat Transfer, Chemical Engineering Progress, Symposium Series, Vol. 55, 1959, p. 103.

12. Corty, C., and Foust, A. S., "Surface Variables in Nucleate Boiling," Heat Transfer, Chemical Engineering Progress, Symposium Series, Vol. 51, 1955, p. 1.

13. Denny, V. E., "Some Effects of Surface Micro-Geometry on Natural Convection and Pool Boiling Heat Transfer to Saturated Carbon Tetrachloride," Ph. D. Thesis, University of Minn., 1961.

14. Drew, T. B. and Hoopes, J. W., Advances in Chemical Engineering, Vol. 1, Academic Press Inc., New York, 1958.

15. Drew, T. B. and Hoopes, J. W., Advances in Chemical Engineering, Vol. 2, Academic Press Inc., New York, 1958.

16. Flynn, T. M., Draper, J. W., and Roos, J. J., "The Nucleate and Film Boiling Curve of Liquid Nitrogen at One Atmosphere," Advances in Cryogenic Engineering, Vol. 7, Plenum Press Inc., New York, 1962, p. 539.

17. Forster, K. E. and Grief, R., "Heat Transfer to a Boiling Liquid, Mechanisms and Correlations," J. Heat Transfer, Vol. 81, Feb. 1959, p. 43.

18. Forster, K. E. and Zuber, N., "Dynamics of Vapor Bubbles and Boiling Heat Transfer," A. I. Ch. E. J., Vol. 1, 1955, p. 531.

19. Frederking, T. H. K., Advances in Cryogenic Engineering, Vol. 8, Plenum Press Inc., New York, 1963, p. 489.

20. Frederking, T. H. K., Personal Communication.

21. Gaertner, R. F., "Photographic Study of Nucleate Pool Boiling on a Horizontal Surface," Paper 63-WA-76, Presented at Meeting of A. S. M. E., Nov. 1963, Philadelphia.

22. Gaertner, R. F , and Westwater, J. W., "Population of Active Sites in Nucleate Boiling Heat Transfer," Heat Transfer, Chemical Engineering Progress, Symposium Series, Vol. 56, 1960, p. 39.

23. Gambill, W., "An Experimental Investigation of the Inherent Uncertainty in Pool-Boiling Critical Heat Fluxes to Saturated Water," Paper Presented at the Symposium on Heat Transfer Part II, San Juan, Puerto Rico, October, 1963.

24. Griffith, P. J. and Wallis, J. D., "The Role of Surface Conditions in Nucleate Boiling," Heat Transfer, Chemical Engineering Progress, Symposium Series, Vol. 56, 1960, p. 49.

25. Guggenheim, E. A., Thermodynamics, North-Holland Publishing Co., Amsterdam, 1959.

26. Haselden, G. G. and Peters, J. I., "Heat Transfer to Boiling Liquid Oxygen and Liquid Nitrogen," Trans. Inst. Chem. Eng., Vol. 27, 1949, p. 201.

27. Hosler, E. R. and Westwater, J. W., A. R. S. J., Vol. 32, 1962, p. 553.

28. Jakob, M., Heat Transfer, Vol. 1, John Wiley & Sons, Inc., New York, 1949.

29. Johnson, V. J., A Compendium of the Properties of Materials at Low Temperature, WADD Technical Report, Part I, 1960.

30. Johnston, H. L., and McClosky, K. E., "Viscosity of Several Common Gases Between 90°K and Room Temperature," J. of Phys. Chem., Vol. 44, 1940, p. 1038.

31. Jones, M. C., Mage, D. T., Faulkner, R. C., and Katz, D. L., "Measurement of Thermodynamic Properties of Gases at Low Temperature and High Pressure-Methane," Thermodynamics, Chemical Engineering Progress, Symposium Series, Vol. 59, 1963, p. 61.

32. Jossi, J. A., Stiel, L. I., and Thodos, G., "The Viscosity of Pure Substances in the Dense Gaseous and Liquid Phases," A. I. Ch. E. J., Vol. 8, March 1962, p. 59.

33. Kutateladze, S. S., Izv. Akad., Nauk., U. S. S. R., O. T. D. Tekh. Nauk, No. 4, 1951, p. 342.

34. Kurihara, H. M. and Myers, J. E., "The Effects of Superheat and Surface Roughness on Boiling Coefficient," A. I. Ch. E. J., Vol. 6, 1960, p. 83.

35. Levy, S., "Generalized Correlation of Boiling Heat Transfer," Journal of Heat Transfer, Vol. 81, Feb. 1949, p. 37.

36. Lienhard, J. H. and Schrock, V. E., "The Effect of Pressure, Geometry, and the Equation of State upon the Peak and Minimum Boiling Heat Flux," J. Heat Transfer, Vol. 85, 1963, p. 261.

37. Lyon, D. N., Kosky, P. G., and Harman, B. N., "Nucleate Boiling Heat Transfer Coefficients and Peak Nucleate Boiling Fluxes for Pure Liquid Nitrogen and Oxygen on Horizontal Platinum Surfaces from 0.5 Atmosphere to the Critical Pressures," Advances in Cryogenic Engineering, Vol. 9, Plenum Press, New York, 1964, p. 77.

38. Mage, D. T., Jones, M. L., Katz, D. L., and Roebuck, J. R., "Experimental Enthalpies for Nitrogen," Thermodynamics, Chemical Engineering Progress, Symposium Series, Vol. 59, 1963, p. 61.

39. Matthews, C. S. and Hurd, C. O., "Thermodynamic Properties of Methane," Trans. Am. Inst. Chem. Eng., Vol. 42, 1946, p. 55.

40. McAdams, W. H., Heat Transmission, Third Ed., McGraw-Hill Book Company, Inc., New York, 1954.

41. McNelly, M. J., "A Correlation of Rates of Heat Transfer to Nucleate Boiling Liquids," J. Imp. Coll. Chem. Eng. Soc., Vol. 7, 1953, p. 18.

42. Moore, F. D. and Mesler, R. B., "The Measurement of Rapid Surface Temperature Fluctuations During Nucleate Boiling of Water," A. I. Ch. E. J., Vol. 7, Dec. 1961, p. 620.

43. Nukiyama, S. J., Soc. Mech. Engr's. (Japan), Vol. 37, 1931, p. 367.

44. Owens, E. J. and Thodos, G., "Reduced Thermal Conductivity Chart for Methane," Proceedings of the Joint Conference on Thermodynamic and Transport Properties of Fluids, The Institute of Mechanical Engineers, London, 1958, p. 163.

45. Owens, E. J., and Thodos, G., "Thermal Conductivity Reduced State Correlation for the Inert Gases," A. I. Ch. E. J., Vol. 3, 1957, p. 454.

46. Perry, J. H., Chemical Engineer's Handbook, McGraw-Hill Company, Inc., New York, 1950, pp. 272-273.

47. Prutton, C. F., and Maron, S. H., Fundamental Principles of Physical Chemistry, The Macmillan Co., New York, 1951.

48. Rohsenow, W. M., Trans. Am. Soc. Mech. Eng. Vol. 74, 1952, p. 969.

49. Rohsenow, W. M. and Griffith, P., "A Correlation of Maximum Heat Flux Data for Boiling of Saturated Liquids," Heat Transfer, Chemical Engineering Progress, Symposium Series, Vol. 52, 1956, p. 47.

50. Roubeau, P., Progress in Refrigeration Science and Technology, Vol. 1, Pergamon Press, New York, 1960, p. 49.

51. Scott, R. B., Cryogenic Engineering, D. Van Nostrand Company, Inc., New York, 1959.

52. Stiel, L. I. and Thodos, G., A. I. Ch. E. J., Vol. 7, 1961, p. 611.

53. Zuber, N., Trans. A. S. M. E., Vol. 80, 1958, p. 711.

APPENDIX A

EXPERIMENTAL DATA

TABLE A-I	NUCLEATE BOILING N_2 DATA ON CLEAN GOLD SURFACE
TABLE A-II	FILM BOILING N_2 DATA ON CLEAN GOLD SURFACE
TABLE A-III	NUCLEATE BOILING CH_4 DATA ON CLEAN GOLD SURFACE
TABLE A-IV	FILM BOILING CH_4 DATA ON CLEAN GOLD SURFACE
TABLE A-V	CONVECTIVE HEAT TRANSFER DATA FOR N_2 NEAR THE CRITICAL POINT
TABLE A-VI	CONVECTIVE HEAT TRANSFER DATA FOR CH_4 NEAR THE CRITICAL POINT
TABLE A-VII	NUCLEATE BOILING N_2 DATA ON COPPER SURFACE
TABLE A-VIII	FILM BOILING N_2 DATA ON COPPER SURFACE
TABLE A-IX	NUCLEATE BOILING N_2 DATA ON FOULED GOLD SURFACE
TABLE A-X	NUCLEATE BOILING CH_4 DATA ON FOULED GOLD SURFACE
TABLE A-XI	FILM BOILING CH_4 DATA ON FOULED GOLD SURFACE

TABLE A-I

NUCLEATE BOILING N_2 DATA ON CLEAN GOLD SURFACE

Run 1 -- Date 4/25/64
Saturation Temperature 139°R
Saturation Pressure 14.5 P.S.I.A.

$Q/A\ (10)^{-4}$ B.t.u./hr. ft.^{2}	ΔT_1 °F	ΔT_2 °F	ΔT_3 °F	h B.t.u./hr. ft.^{2} °F
0.211	3.9	3.9	3.9	341
0.634	5.4	6.1	6.1	1039
1.291	6.8	7.2	7.2	1793
2.549	7.9	8.9	8.9	2864
3.458	8.6	9.6	9.6	3602
3.586	8.9	9.6	9.6	3735
3.717	9.1	9.9	9.9	3754
3.804	9.1	9.9	9.9	3842
3.977	9.3	9.9	9.9	4017
4.157	9.7	9.9	9.9	4198
4.244	10.0	10.7	10.7	3966
4.428	10.0	11.4	11.4	3881
4.517	Burnout Point			

Run 2 -- Date 4/26/64
Saturation Temperature 139°R
Saturation Pressure 14.5 P.S.I.A.

$Q/A\ (10)^{-4}$ B.t.u./hr. ft.^{2}	ΔT_1 °F	ΔT_2 °F	ΔT_3 °F	h B.t.u./hr. ft.^{2} °F
0.177	2.8	3.2	3.2	553
0.316	3.6	4.3	4.3	735
1.977	6.5	7.5	7.5	2636
3.002	7.5	8.6	8.6	3490
3.914	8.6	10.0	10.0	3914
4.165	9.7	10.7	10.7	3893
4.331	Burnout Point			

TABLE A-I continued

Run 3 -- Date 4/26/64
Saturation Temperature 139°R
Saturation Pressure 14.5 P.S.I.A.

$Q/A\ (10)^{-4}$ B.t.u./hr. ft.^{2}	ΔT_1 °F	ΔT_2 °F	ΔT_3 °F	h B.t.u./hr. ft.^{2} °F
0.247	3.6	3.9	3.9	633
1.287	6.5	7.5	7.5	1716
2.309	7.5	9.0	9.0	2565
3.163	8.3	10.0	10.0	3163
4.006	9.7	11.4	11.4	3514
4.222	Burnout Point			

Run 4 -- Date 4/26/64
Saturation Temperature 139°R
Saturation Pressure 14.5 P.S.I.A.

$Q/A\ (10)^{-4}$ B.t.u./hr. ft.^{2}	ΔT_1 °F	ΔT_2 °F	ΔT_3 °F	h B.t.u./hr. ft.^{2} °F
0.184	2.8	3.6	3.6	511
1.808	6.1	7.9	7.9	2288
3.756	9.7	10.7	10.7	3510
4.139	Burnout Point			

Run 5 -- Date 5/12/64
Saturation Temperature 166°R
Saturation Pressure 64 P.S.I.A.

$Q/A\ (10)^{-4}$ B.t.u./hr. ft.^{2}	ΔT_1 °F	ΔT_2 °F	ΔT_3 °F	h B.t.u./hr. ft.^{2} °F
0.205	2.2	2.9	2.9	707
0.978	3.6	4.3	4.3	2274
2.467	4.7	5.4	5.4	4568
3.458	5.4	6.4	6.4	5403
4.481	6.4	8.2	8.2	5464
5.078	6.8	8.6	8.6	5904
5.440	Burnout Point			

TABLE A-I continued

Run 6 -- Date 5/15/64
Saturation Temperature 179°R
Saturation Pressure 114 P.S.I.A.

$Q/A\ (10)^{-4}$ B.t.u./hr. ft.^{2}	ΔT_1 °F	ΔT_2 °F	ΔT_3 °F	h B.t.u./hr. ft.^{2} °F
0.240	1.3	1.7	1.7	1412
2.314	4.0	4.7	4.7	4923
3.501	4.7	6.0	6.0	5835
5.440	6.0	8.0	8.0	6800
5.803	6.7	8.3	8.3	6991
5.982	Burnout Point			

Run 7 -- Date 5/10/64
Saturation Temperature 187°R
Saturation Pressure 148 P.S.I.A.

$Q/A\ (10)^{-4}$ B.t.u./hr. ft.^{2}	ΔT_1 °F	ΔT_2 °F	ΔT_3 °F	h B.t.u./hr. ft.^{2} °F
0.209	1.6	1.6	1.6	
1.398	3.1	4.4	3.6	
2.372	3.8	4.7	4.7	

Run 8 -- Date 5/12/64
Saturation Temperature 187°R
Saturation Pressure 148 P.S.I.A.

$Q/A\ (10)^{-4}$ B.t.u./hr. ft.^{2}	ΔT_1 °F	ΔT_2 °F	ΔT_3 °F	h B.t.u./hr. ft.^{2} °F
0.195	1.6	1.9	1.9	1026
1.059	2.5	3.1	3.1	3416
2.404	3.8	4.4	4.4	5463
3.850	4.4	5.0	5.0	7700
4.118	5.0	5.3	5.3	7769

TABLE A-I continue

Run 9* -- Date 5/12
Saturation Temperature
Saturation Pressure 214

$Q/A\ (10)^{-4}$ B.t.u./hr. ft.^{2}	ΔT_1 °F	ΔT_2 °F	ΔT °F
0.220	0.9	1.4	1.
0.797	1.6	2.4	2.
2.344	2.4	3.5	3.
2.615	2.7	3.5	3.
2.699	2.7	3.5	3.
2.904	2.7	3.5	3.
3.112	3.0	3.8	3.
3.285	3.0	3.8	3.
3.501	3.3	4.1	4.
3.808	3.3	4.1	4.
3.941	3.5	4.4	4.
4.257	3.7	4.7	4.
4.534	3.8	4.7	4.
4.715	3.8	4.7	4.
4.896	4.1	5.3	5.
5.078	4.4	5.9	5.
5.440	4.4	6.2	6.
5.984	5.3	7.1	7.
6.166	7.4	7.7	7.
6.347	7.4	7.7	7
6.529	Burnout Point		

Run 10 -- Date 5/11
Saturation Temperature
Saturation Pressure 214

$Q/A\ (10)^{-4}$ B.t.u./hr. ft.^{2}	ΔT_1 °F	ΔT_2 °F	ΔT °F
0.261	1.6	2.1	2.
2.531	3.8	4.4	4.
4.500	4.1	4.7	4.
5.693	5.3	6.0	6.
5.978	Burnout Point		

*Note this run was interrupted
this gave a high critical flux.

TABLE A-I continued

Run 9* -- Date 5/12/64
Saturation Temperature 198°R
Saturation Pressure 214 P.S.I.A.

$Q/A\ (10)^{-4}$ B.t.u./hr. ft.^{2}	ΔT_1 °F	ΔT_2 °F	ΔT_3 °F	h B.t.u./hr. ft.^{2} °F
0.220	0.9	1.4	1.4	1571
0.797	1.6	2.4	2.4	3321
2.344	2.4	3.5	3.5	6697
2.615	2.7	3.5	3.5	7471
2.699	2.7	3.5	3.5	7711
2.904	2.7	3.5	3.5	8297
3.112	3.0	3.8	3.8	8189
3.285	3.0	3.8	3.8	8644
3.501	3.3	4.1	4.1	8539
3.808	3.3	4.1	4.1	9287
3.941	3.5	4.4	4.4	8956
4.257	3.7	4.7	4.7	9057
4.534	3.8	4.7	4.7	9646
4.715	3.8	4.7	4.7	10031
4.896	4.1	5.3	5.3	9237
5.078	4.4	5.9	5.9	8606
5.440	4.4	6.2	6.2	8774
5.984	5.3	7.1	7.1	8428
6.166	7.4	7.7	7.7	8007
6.347	7.4	7.7	7.7	8242
6.529	Burnout Point			

Run 10 -- Date 5/11/64
Saturation Temperature 198°R
Saturation Pressure 214 P.S.I.A.

$Q/A\ (10)^{-4}$ B.t.u./hr. ft.^{2}	ΔT_1 °F	ΔT_2 °F	ΔT_3 °F	h B.t.u./hr. ft.^{2} °F
0.261	1.6	2.1	2.1	1243
2.531	3.8	4.4	4.4	5752
4.500	4.1	4.7	4.7	9574
5.693	5.3	6.0	6.0	9488
5.978	Burnout Point			

*Note this run was interrupted and started at 30 volts this gave a high critical flux.

TABLE A-I continued

Run 11 -- Date 5/15/64
Saturation Temperature 209°R
Saturation Pressure 299 P.S.I.A.

$Q/A\ (10)^{-4}$ B.t.u./hr. ft.^{2}	ΔT_1 °F	ΔT_2 °F	ΔT_3 °F	h B.t.u./hr. ft.^{2} °F
0.234	1.4	1.7	1.7	1376
1.398	1.7	2.6	2.6	5376
2.435	2.0	2.9	2.9	8396
2.994	2.0	2.9	2.9	10324
3.205	2.3	3.1	3.1	10338
3.416	2.4	3.4	3.4	10047
3.587	2.4	3.5	3.5	10248
3.847	2.9	4.0	4.0	9617
4.193	3.4	4.6	4.6	9115
4.323	4.0	5.1	5.1	8476
4.551	5.1	6.3	5.7	7984
4.726	Burnout Point			

Run 12 -- Date 5/21/64
Saturation Temperature 219°R
Saturation Pressure 389 P.S.I.A.

$Q/A\ (10)^{-4}$ B.t.u./hr. ft.^{2}	ΔT_1 °F	ΔT_2 °F	ΔT_3 °F	h B.t.u./hr. ft.^{2} °F
0.261	0.8	1.1	1.1	2373
1.434	1.4	1.7	1.7	8435
2.444	1.9	2.5	2.5	9776
3.002	2.5	3.5	3.5	8577
3.122	Burnout Point			

Run 13 -- Date 6/13/64
Saturation Temperature 219°R
Saturation Pressure 387 P.S.I.A.

$Q/A\ (10)^{-4}$ B.t.u./hr. ft.^{2}	ΔT_1 °F	ΔT_2 °F	ΔT_3 °F	h B.t.u./hr. ft.^{2} °F
1.347	0.05	1.4	---	9621
2.249	0.08	2.2	---	10222
3.026	Burnout Point			

TABLE A-I continued

Run 14 -- Date 6/13/64
Saturation Temperature 219°R
Saturation Pressure 398 P.S.I.A.

$Q/A\ (10)^{-4}$ B.t.u./hr. ft.^{2}	ΔT_1 °F	ΔT_2 °F	ΔT_3 °F	h B.t.u./hr. ft.^{2} °F
1.480	1.1	2.2	---	6727
1.963	1.4	2.8	---	7010
2.362	1.7	3.6	---	6561
3.083	Burnout Point			

Run 15 -- Date 5/10/64
Saturation Temperature 223°R
Saturation Pressure 442 P.S.I.A.

$Q/A\ (10)^{-4}$ B.t.u./hr. ft.^{2}	ΔT_1 °F	ΔT_2 °F	ΔT_3 °F	h B.t.u./hr. ft.^{2} °F
0.219	0.5	0.5	0.5	4380
0.329	0.75	0.75	0.75	4386
0.408	1.0	1.0	1.0	4080
0.474	Burnout Point			

Run 16 -- Date 5/21/64
Saturation Temperature 223°R
Saturation Pressure 442 P.S.I.A.

$Q/A\ (10)^{-4}$ B.t.u./hr. ft.^{2}	ΔT_1 °F	ΔT_2 °F	ΔT_3 °F	h B.t.u./hr. ft.^{2} °F
0.261	0.65	0.65	0.65	4015
0.412	1.1	1.1	1.1	3745
0.474	1.1	1.1	1.1	4309
0.497	Burnout Point			

TABLE A-II

FILM BOILING N_2 DATA ON CLEAN GOLD SURFACE

Run 17 -- Date 4/25/64
Saturation Temperature 139°R
Saturation Pressure 14.5 P.S.I.A.

$Q/A\ (10)^{-4}$ B.t.u./hr. ft.^{2}	ΔT_1 °F	ΔT_2 °F	ΔT_3 °F	h B.t.u./hr. ft.^{2} °F
1.502	365	364	363	41.3
2.277	584	584	581	39.1
0.966	252	252	251	38.3

Run 18 -- Date 4/26/64
Saturation Temperature 129°R
Saturation Pressure 14.5 P.S.I.A.

$Q/A\ (10)^{-4}$ B.t.u./hr. ft.^{2}	ΔT_1 °F	ΔT_2 °F	ΔT_3 °F	h B.t.u./hr. ft.^{2} °F
0.886	203	201	200	44.1
0.485	89	89	89	54.5
1.608	359	359	356	45.0
3.270	884	880	878	37.1

Run 19 -- Date 4/26/64
Saturation Temperature 139°R
Saturation Pressure 14.5 P.S.I.A.

$Q/A\ (10)^{-4}$ B.t.u./hr. ft.^{2}	ΔT_1 °F	ΔT_2 °F	ΔT_3 °F	h B.t.u./hr. ft.^{2} °F
0.7275	168	167	167	43.6

TABLE A-II continued

Date 5/21/64
Saturation Temperature 179°R
Saturation Pressure 114 P.S.I.A.

$Q/A\ (10)^{-4}$ B.t.u./hr. ft.^{2}	ΔT_1 °F	ΔT_2 °F	ΔT_3 °F	h B.t.u./hr. ft.^{2} °F
1.833	210	210	210	87.3
1.634	154	154	154	106.1

Run 20 -- Date 5/15/64
Saturation Temperature 184°R
Saturation Pressure 148 P.S.I.A.

$Q/A\ (10)^{-4}$ B.t.u./hr. ft.^{2}	ΔT_1 °F	ΔT_2 °F	ΔT_3 °F	h B.t.u./hr. ft.^{2} °F
1.961	218	217	219	90.0
1.608	143	143	143	112.4
2.115	275	274	275	76.9

Run 21 -- Date 5/15/64
Saturation Temperature 198°R
Saturation Pressure 214 P.S.I.A.

$Q/A\ (10)^{-4}$ B.t.u./hr. ft.^{2}	ΔT_1 °F	ΔT_2 °F	ΔT_3 °F	h B.t.u./hr. ft.^{2} °F
2.446	338	336	338	72.5
1.990	238	237	238	83.6
1.576	145	144	145	108.7
1.372	76	75	76	180.5

TABLE A-II continued

Run 22 -- Date 5/15/64
Saturation Temperature 209°R
Saturation Pressure 299 P.S.I.A.

$Q/A\ (10)^{-4}$ B.t.u./hr. ft.^{2}	ΔT_1 °F	ΔT_2 °F	ΔT_3 °F	h B.t.u./hr. ft.^{2} °F
1.040	54	54	54	192.6
1.893	232	233	234	81.2
2.446	324	324	326	75.5
2.691	363	366	367	73.7

Run 23 -- Date 5/21/64
Saturation Temperature 219°R
Saturation Pressure 389 P.S.I.A.

$Q/A\ (10)^{-4}$ B.t.u./hr. ft.^{2}	ΔT_1 °F	ΔT_2 °F	ΔT_3 °F	h B.t.u./hr. ft.^{2} °F
3.110	410	407	411	76.2
2.385	314	312	315	76.2
1.834	227	225	227	81.2
1.472	171	171	172	86.1
1.181	126	126	126	93.7
0.928	81	81	81	114.6

Run 24 -- Date 5/10/64
Saturation Temperature 223°R
Saturation Pressure 442 P.S.I.A.

$Q/A\ (10)^{-4}$ B.t.u./hr. ft.^{2}	ΔT_1 °F	ΔT_2 °F	ΔT_3 °F	h B.t.u./hr. ft.^{2} °F
0.502	174	174	174	28.8
1.616	495	494	497	32.6
1.181	392	391	393	30.1
1.815	587	583	589	63.0
0.702	257	256	258	27.3
0.379	141	141	141	26.9

TABLE A-III

NUCLEATE BOILING CH_4 DATA ON CLEAN GOLD SURFACE

Run 25 -- Date 6/17/64
Saturation Temperature 260°R
Saturation Pressure 114 P.S.I.A.

$Q/A\ (10)^{-4}$ B.t.u./hr. ft.^{2}	ΔT_1 °F	ΔT_2 °F	ΔT_3 °F	h B.t.u./hr. ft.^{2} °F
1.392	10.0	10.5	10.5	1326
1.924	12.2	13.0	13.0	1480
2.242	14.6	16.2	16.2	1384
2.549	15.6	18.5	18.5	1379
2.868	19.0	20.0	20.0	1434

Run 26 -- Date 6/17/64
Saturation Temperature 286°R
Saturation Pressure 214 P.S.I.A.

$Q/A\ (10)^{-4}$ B.t.u./hr. ft.^{2}	ΔT_1 °F	ΔT_2 °F	ΔT_3 °F	h B.t.u./hr. ft.^{2} °F
1.357	6.9	8.2	8.2	1654
1.911	11.7	12.6	12.6	1517
2.262	13.4	14.1	13.9	1627
2.344	14.5	15.2	15.2	1542
2.457	15.2	15.7	15.6	1575

TABLE A-III continued

Run 27 -- Date 6/17/64
Saturation Temperature 303°R
Saturation Pressure 314 P.S.I.A.

$Q/A\ (10)^{-4}$ B.t.u./hr. ft.^{2}	ΔT_1 °F	ΔT_2 °F	ΔT_3 °F	h B.t.u./hr. ft.^{2} °F
1.307	6.5	7.2	7.2	1825
1.632	8.7	9.3	9.3	1754
2.030	10.4	11.1	11.3	1796
2.277	11.5	12.2	12.2	1866
2.594	12.8	14.4	14.4	1806
3.174	15.8	16.5	16.5	1924
3.619	18.0	18.7	18.7	1935
3.804	18.7	19.5	19.5	1951
3.897	20.0	20.4	20.4	1910
4.223	21.5	22.1	22.0	1920

Run 28 -- Date 6/17/64
Saturation Temperature 317°R
Saturation Pressure 414 P.S.I.A.

$Q/A\ (10)^{-4}$ B.t.u./hr. ft.^{2}	ΔT_1 °F	ΔT_2 °F	ΔT_3 °F	h B.t.u./hr. ft.^{2} °F
1.290	6.9	7.1	7.1	1806
1.638	8.3	9.0	9.0	1830
2.109	10.2	10.9	10.9	1935
2.688	12.1	13.1	13.1	2052
3.284	14.5	15.9	15.9	2065
3.838	17.6	19.0	19.0	2020
3.977	18.6	19.5	19.5	2039

Run 29 -- Date 6/17/64
Saturation Temperature 260°R
Saturation Pressure 114 P.S.I.A.

$Q/A\ (10)^{-4}$ B.t.u./hr. ft.^{2}	ΔT_1 °F	ΔT_2 °F	ΔT_3 °F	h B.t.u./hr. ft.^{2} °F
1.434	10.6	11.5	---	1247
1.845	11.3	12.2	---	1512
2.404	15.2	19.0	---	1265

TABLE A-III continued

Run 30 -- Date 6/17/64
Saturation Temperature 328°R
Saturation Pressure 514 P.S.I.A.

$Q/A\ (10)^{-4}$ B.t.u./hr. ft.^{2}	ΔT_1 °F	ΔT_2 °F	ΔT_3 °F	h B.t.u./hr. ft.^{2} °F
1.181	6.2	6.8	6.9	1736
1.813	8.8	9.5	9.6	1908
2.358	10.8	12.0	12.0	1965
3.070	13.5	14.5	14.5	2117
3.481	14.8	16.2	16.0	2149

TABLE A-IV

FILM BOILING CH_4 DATA ON CLEAN GOLD SURFACE

Run 31 -- Date 6/17/64
Saturation Temperature 212°R
Saturation Pressure 24 P.S.I.A.

$Q/A\ (10)^{-4}$ B.t.u./hr. ft.^{2}	ΔT_1 °F	ΔT_2 °F	ΔT_3 °F	h B.t.u./hr. ft.^{2} °F
1.679	584	585	---	28.5
1.773	764	768	---	23.4

Run 32 -- Date 6/17/64
Saturation Temperature 260°R
Saturation Pressure 114 P.S.I.A.

$Q/A\ (10)^{-4}$ B.t.u./hr. ft.^{2}	ΔT_1 °F	ΔT_2 °F	ΔT_3 °F	h B.t.u./hr. ft.^{2} °F
1.619	361	362	---	44.7
2.178	620	621	---	35.1
2.796	795	802	---	35.0
1.864	565	574	---	32.7

Run 33 -- Date 6/17/64
Saturation Temperature 286°R
Saturation Pressure 214 P.S.I.A.

$Q/A\ (10)^{-4}$ B.t.u./hr. ft.^{2}	ΔT_1 °F	ΔT_2 °F	ΔT_3 °F	h B.t.u./hr. ft.^{2} °F
4.875	875	885	---	55.4
3.981	784	794	---	50.5
2.834	607	613	---	46.5
2.320	510	514	---	45.1
1.699	394	397	---	42.9

TABLE A-IV continued

Run 34 -- Date 6/17/64
Saturation Temperature 303°R
Saturation Pressure 314 P.S.I.A.

$Q/A\ (10)^{-4}$ B.t.u./hr. ft.^{2}	ΔT_1 °F	ΔT_2 °F	ΔT_3 °F	h B.t.u./hr. ft.^{2} °F
5.398	801	805	---	67.2
3.987	662	667	---	60.0
3.234	591	597	---	54.4
1.651	293	295	---	56.2

Run 35 -- Date 6/17/64
Saturation Temperature 303°R
Saturation Pressure 314 P.S.I.A.

$Q/A\ (10)^{-4}$ B.t.u./hr. ft.^{2}	ΔT_1 °F	ΔT_2 °F	ΔT_3 °F	h B.t.u./hr. ft.^{2} °F
5.345	701	704	---	76.1
4.091	579	582	---	70.7
2.568	452	454	---	56.7
1.651	273	274	---	60.4

Run 36 -- Date 6/17/64
Saturation Temperature 317°R
Saturation Pressure 414 P.S.I.A.

$Q/A\ (10)^{-4}$ B.t.u./hr. ft.^{2}	ΔT_1 °F	ΔT_2 °F	ΔT_3 °F	h B.t.u./hr. ft.^{2} °F
5.331	704	707	---	75.6
3.985	572	577	---	69.4
2.691	435	438	---	61.4
1.585	274	275	---	57.7

TABLE A-IV continued

Run 37 -- Date 6/17/64
Saturation Temperature 328°R
Saturation Pressure 514 P.S.I.A.

$Q/A\ (10)^{-4}$ B.t.u./hr. ft.^{2}	ΔT_1 °F	ΔT_2 °F	ΔT_3 °F	h B.t.u./hr. ft.^{2} °F
6.054	732	739	---	82.3
4.993	662	667	---	75.2
3.416	516	518	---	66.1
2.184	368	369	---	59.3
1.676	299	300	---	55.9

Run 38 -- Date 6/17/64
Saturation Temperature 339°R
Saturation Pressure 614 P.S.I.A.

$Q/A\ (10)^{-4}$ B.t.u./hr. ft.^{2}	ΔT_1 °F	ΔT_2 °F	ΔT_3 °F	h B.t.u./hr. ft.^{2} °F
5.938	844	850	---	69.7
4.049	634	635	---	63.8
2.813	472	472	---	59.6
2.332	400	402	---	58.2
1.788	320	321	---	55.8
1.645	304	305	---	53.9

TABLE A-V

CONVECTIVE HEAT TRANSFER DATA N_2 NEAR THE CRITICAL POINT

*Run 39 -- Date 7/5/64
Bulk Temperature 227°R
Pressure 492 P.S.I.A.

$Q/A\ (10)^{-4}$ B.t.u./hr. ft.^{2}	ΔT_1 °F	ΔT_2 °F	ΔT_3 °F	h B.t.u./hr. ft.^{2} °F
1.708	170	160	164	104.1
2.187	229	225	229	95.9
2.745	294	336	331	85.8

Run 40 -- Date 7/5/64
Bulk Temperature 227°R
Pressure 514 P.S.I.A.

$Q/A\ (10)^{-4}$ B.t.u./hr. ft.^{2}	ΔT_1 °F	ΔT_2 °F	ΔT_3 °F	h B.t.u./hr. ft.^{2} °F
2.757	290	286	287	95.7
2.222	216	212	215	103.8
1.896	163	162	162	117.0
1.704	141	138	138	122.6

Run 41 -- Date 7/5/64
Bulk Temperature 227°R
Pressure 614 P.S.I.A.

$Q/A\ (10)^{-4}$ B.t.u./hr. ft.^{2}	ΔT_1 °F	ΔT_2 °F	ΔT_3 °F	h B.t.u./hr. ft.^{2} °F
1.700	136	133	135	125.9
2.391	226	221	225	106.7
2.969	310	303	308	96.7
3.374	377	370	372	90.5

*Note: Temperature was fluctuating badly and these are average readings.

TABLE A-V continued

Run 42 -- Date 7/5/64
Bulk temperature 227°R
Pressure 719 P.S.I.A.

$Q/A\ (10)^{-4}$ B.t.u./hr. ft.^{2}	ΔT_1 °F	ΔT_2 °F	ΔT_3 °F	h B.t.u./hr. ft.^{2} °F
1.699	134	132	134	127.7
2.801	268	265	268	104.9
3.340	347	344	348	96.5
2.362	211	210	210	112.5

Run 43 -- Date 7/5/64
Bulk temperature 227°R
Pressure 814 P.S.I.A.

$Q/A\ (10)^{-4}$ B.t.u./hr. ft.^{2}	ΔT_1 °F	ΔT_2 °F	ΔT_3 °F	h B.t.u./hr. ft.^{2} °F
1.668	142	138	142	118.3
2.424	233	229	233	104.5
2.856	295	289	292	97.8
3.374	374	372	372	90.5

TABLE A-VI

CONVECTIVE HEAT TRANSFER DATA FOR CH_4 NEAR THE CRITICAL POINT

Run 44 -- Date 7/7/64
Bulk Temperature 344°R
Pressure 714 P.S.I.A.

$Q/A\ (10)^{-4}$ B.t.u./hr. ft.^{2}	ΔT_1 °F	ΔT_2 °F	ΔT_3 °F	h B.t.u./hr. ft.^{2} °F
2.688	238.5	234	236	113.9
2.079	162	160	162	129.1
1.731	107	106	107	161.8
2.331	189	186	188	124.5

Run 45 -- Date 7/7/64
Bulk Temperature 344°R
Pressure 764 P.S.I.A.

$Q/A\ (10)^{-4}$ B.t.u./hr. ft.^{2}	ΔT_1 °F	ΔT_2 °F	ΔT_3 °F	h B.t.u./hr. ft.^{2} °F
2.467	185	182	183	134.8
2.146	151	146	149	144.0
1.833	121	118	120	154.0

Run 46 -- Date 7/7/64
Bulk Temperature 344°R
Pressure 814 P.S.I.A.

$Q/A\ (10)^{-4}$ B.t.u./hr. ft.^{2}	ΔT_1 °F	ΔT_2 °F	ΔT_3 °F	h B.t.u./hr. ft.^{2} °F
2.615	193.3	188	191	136.9
2.271	163.1	158	162	141.0
2.048	139.2	136	137	149.5
1.742	110	108	110	159.8

TABLE A-VI continued

Run 47 -- Date 7/7/64
Bulk Temperature 344°R
Pressure 864 P.S.I.A.

$Q/A\ (10)^{-4}$ B.t.u./hr. ft.^{2}	ΔT_1 °F	ΔT_2 °F	ΔT_3 °F	h B.t.u./hr. ft.^{2} °F
2.435	178	173	175	139.1
2.240	157	153	156	144.5
2.110	148	144	147	144.5
1.742	110	106	108	161.3

TABLE A-VII

NUCLEATE BOILING N_2 DATA ON A COPPER SURFACE

Run 48 -- Date 5/10/64
Saturation Temperature 139°R
Saturation Pressure 14.2 P.S.I.A.

$Q/A\ (10)^{-4}$ B.t.u./hr. ft.^{2}	ΔT_1 °F	ΔT_2 °F	ΔT_3 °F	h B.t.u./hr. ft.^{2} °F
0.209	---	9.0	---	
0.390	---	13.5	---	
0.783	---	18.9	---	
1.851	---	27.0	---	
3.440	---	37.8	---	
3.960	---	37.8	---	
4.184	---	38.7	---	
4.370	---	39.6	---	
4.596	Burnout Point			

Run 49 -- Date 5/10/64
Saturation Temperature 139°R
Saturation Pressure 14.2 P.S.I.A.

$Q/A\ (10)^{-4}$ B.t.u./hr. ft.^{2}	ΔT_1 °F	ΔT_2 °F	ΔT_3 °F	h B.t.u./hr. ft.^{2} °F
0.259	---	7.0	---	
0.643	---	8.0	---	
1.385	---	18.0	---	
1.690	---	26.9	---	
2.209	---	28.0	---	
2.440	---	28.4	---	
4.060	---	28.5	---	
4.406	---	28.6	---	
4.500	Burnout Point			

TABLE A-VII continued

Run 50 -- Date 5/10/64
Saturation Temperature 139°R
Saturation Pressure 14.2 P.S.I.A.

$Q/A\ (10)^{-4}$ B.t.u./hr. ft.^{2}	ΔT_1 °F	ΔT_2 °F	ΔT_3 °F	h B.t.u./hr. ft.^{2} °F
0.225	---	3.9	---	
0.551	---	8.6	---	
1.838	---	17.3	---	
5.34	---	33.3	---	
5.73	Burnout Point			

TABLE A-VIII

FILM BOILING N_2 DATA ON A COPPER SURFACE

Run 51 -- Date 5/10/64
Saturation Temperature 139°R
Saturation Pressure 14.2 P.S.I.A.

$Q/A\ (10)^{-4}$ B.t.u./hr. ft.^{2}	ΔT_1 °F	ΔT_2 °F	ΔT_3 °F	h B.t.u./hr. ft.^{2} °F
0.659	---	152	---	
1.594	---	283	---	
2.231	---	464	---	
3.000	---	704	---	
3.550	---	1009	---	
4.470	---	76	---	

Run 52 -- Date 5/10/64
Saturation Temperature 139°R
Saturation Pressure 14.2 P.S.I.A.

$Q/A\ (10)^{-4}$ B.t.u./hr. ft.^{2}	ΔT_1 °F	ΔT_2 °F	ΔT_3 °F	h B.t.u./hr. ft.^{2} °F
0.631	---	124	---	
1.090	---	250	---	
1.566	---	376	---	
1.854	---	402	---	

Run 53 -- Date 5/10/64
Saturation Temperature 139°R
Saturation Pressure 14.2 P.S.I.A.

$Q/A\ (10)^{-4}$ B.t.u./hr. ft.^{2}	ΔT_1 °F	ΔT_2 °F	ΔT_3 °F	h B.t.u./hr. ft.^{2} °F
2.190	---	458	---	
2.238	---	564	---	
2.460	---	619	---	

TABLE A-IX

NUCLEATE BOILING N_2 DATA ON FOULED GOLD SURFACE

Run 54 -- Date 7/5/64
Saturation Temperature 219°R
Saturation Pressure 389 P.S.I.A.

$Q/A\ (10)^{-4}$ B.t.u./hr. ft.^{2}	ΔT_1 °F	ΔT_2 °F	ΔT_3 °F	h B.t.u./hr. ft.^{2} °F
1.476	4.7	4.7	4.7	3140
1.727	6.1	6.4	6.4	2698
2.741	6.4	6.7	6.7	4091
3.069	6.9	7.5	7.5	4092
3.242	7.1	7.8	7.8	4156
3.457	7.4	7.8	7.8	4576
3.676	7.8	8.1	8.1	4538
3.808	Burnout Point			

TABLE A-X

NUCLEATE BOILING CH_4 DATA ON FOULED GOLD SURFACE

Run 55 -- Date 7/1/64
Saturation Temperature 212°R
Saturation Pressure 24 P.S.I.A.

$Q/A\ (10)^{-4}$ B.t.u./hr. ft.^{2}	ΔT_1 °F	ΔT_2 °F	ΔT_3 °F	h B.t.u./hr. ft.^{2} °F
0.247	5.2	5.2	5.2	475
0.569	8.4	8.8	8.8	6465
2.412	13.1	13.2	13.2	1827
4.063	15.0	15.2	15.2	2673
4.216	15.2	15.5	15.5	2720
4.412	15.5	15.8	15.8	2792
4.706	15.5	15.8	15.8	2978

Run 56 -- Date 7/1/64
Saturation Temperature 212°R
Saturation Pressure 24 P.S.I.A.

$Q/A\ (10)^{-4}$ B.t.u./hr. ft.^{2}	ΔT_1 °F	ΔT_2 °F	ΔT_3 °F	h B.t.u./hr. ft.^{2} °F
3.542	15.0	15.5	15.5	2285
4.639	16.9	17.5	17.5	2651
5.692	17.9	18.5	18.5	3077
6.140	18.4	18.8	18.8	3266

TABLE A-X continued

Run 57 -- Date 7/3/64
Saturation Temperature 334°R
Saturation Pressure 564 P.S.I.A.

$Q/A\ (10)^{-4}$ B.t.u./hr. ft.^{2}	ΔT_1 °F	ΔT_2 °F	ΔT_3 °F	h B.t.u./hr. ft.^{2} °F
1.497	11	11.8	11.8	1269
3.851	16.3	17.3	17.3	2226
4.692	18.3	19.5	19.5	2406
5.818	18.7	20.3	20.3	2866
7.676	20.7	22.7	22.7	3381
7.865	22.7	23.5	23.5	3347
8.059	24.2	24.7	24.7	3263
8.443	25.0	26.0	26.0	3247
8.636	26.2	27.0	27.0	3198
8.827	26.5	27.5	27.5	3210
9.211	27.5	27.7	27.7	3325
9.595	28.0	28.5	28.5	3367
10.088	28.5	29.0	29.0	3478
10.282	29.0	29.3	29.3	3509
10.476	Burnout Point			

Run 58 -- Date 7/3/64
Saturation Temperature 310°R
Saturation Pressure 364 P.S.I.A.

$Q/A\ (10)^{-4}$ B.t.u./hr. ft.^{2}	ΔT_1 °F	ΔT_2 °F	ΔT_3 °F	h B.t.u./hr. ft.^{2} °F
1.766	17.4	18.0	18.0	981
4.217	31.1	33.5	33.5	1259
5.313	39.0	40.5	40.5	1312
7.591	45.0	46.3	46.3	1640
9.489	52.5	53.0	53.0	1790
10.476	55.7	56.3	56.3	1860

TABLE A-X continued

Run 59 -- Date 7/3/64
Saturation Temperature 272°R
Saturation Pressure 164 P.S.I.A.

$Q/A\ (10)^{-4}$ B.t.u./hr. ft.^{2}	ΔT_1 °F	ΔT_2 °F	ΔT_3 °F	h B.t.u./hr. ft.^{2} °F
1.797	17.9	18.8	18.8	965
2.309	19.4	20.2	20.2	1130
2.863	21.7	21.8	21.8	1310
3.414	23.1	23.2	23.2	1470
3.938	24.5	24.8	24.8	1590
3.458	22.4	22.5	22.5	1540
2.915	20.1	20.5	20.5	1420
2.404	18.3	18.5	18.5	1300
1.797	15.3	15.5	15.5	1150

Run 60 -- Date 7/3/64
Saturation Temperature 272°R
Saturation Pressure 164 P.S.I.A.

$Q/A\ (10)^{-4}$ B.t.u./hr. ft.^{2}	ΔT_1 °F	ΔT_2 °F	ΔT_3 °F	h B.t.u./hr. ft.^{2} °F
1.502	21.5	22.2	22.2	680
2.404	23.1	23.2	23.2	1020
3.938	22.9	23.4	23.4	1680
3.416	24.8	25.2	25.2	1360
3.938	26.8	27.1	27.1	1430
3.416	23.4	23.1	23.1	1470
2.915	21.7	21.7	21.7	1330
2.404	19.0	19.0	19.0	1270
1.797	15.5	15.5	15.5	1180

TABLE A-X continued

Run 61 -- Date 7/7/64
Saturation Temperature 303°R
Saturation Pressure 314 P.S.I.A.

$Q/A\ (10)^{-4}$ B.t.u./hr. ft.^{2}	ΔT_1 °F	ΔT_2 °F	ΔT_3 °F	h B.t.u./hr. ft.^{2} °F
1.610	18.5	18.5	18.5	870
2.604	21.5	22.0	22.0	1185
5.567	31.0	31.3	31.3	1779

Run 62 -- Date 7/6/64
Saturation Temperature 339°R
Saturation Pressure 614 P.S.I.A.

$Q/A\ (10)^{-4}$ B.t.u./hr. ft.^{2}	ΔT_1 °F	ΔT_2 °F	ΔT_3 °F	h B.t.u./hr. ft.^{2} °F
1.512	16.5	18.5	18.5	817
2.391	22.7	23.3	25.0	1026
2.405	22.7	23.3	25.0	1032
2.809	25.0	26.5	27.5	1060

Run 63 -- Date 7/7/64
Saturation Temperature 310°R
Saturation Pressure 364 P.S.I.A.

$Q/A\ (10)^{-4}$ B.t.u./hr. ft.^{2}	ΔT_1 °F	ΔT_2 °F	ΔT_3 °F	h B.t.u./hr. ft.^{2} °F
1.576	21.0	21.7	21.7	726
1.956	23.0	22.5	22.5	869
2.452	26.0	24.7	24.7	993
3.247	30.0	30.8	30.8	1054
3.938	33.7	34.3	34.3	1148
4.660	40.0	40.5	40.5	1151

TABLE A-X continued

Run 64 -- Date 7/17/64
Saturation Temperature 342.5°R
Saturation Pressure 664 P.S.I.A.

$Q/A\ (10)^{-4}$ B.t.u./hr. ft.^{2}	ΔT_1 °F	ΔT_2 °F	ΔT_3 °F	h B.t.u./hr. ft.^{2} °F
1.594	33.2	36.0	36.0	443
2.151	31.0	33.3	33.3	646
2.151	28.0	31.7	31.7	678
2.151	Burnout point after about 30 minutes			

TABLE A-XI

FILM BOILING CH_4 DATA ON FOULED GOLD SURFACE

Run 65 -- Date 7/13/64
Saturation Temperature 334°R
Saturation Pressure 564 P.S.I.A.

$Q/A\ (10)^{-4}$ B.t.u./hr. ft.^{2}	ΔT_1 °F	ΔT_2 °F	ΔT_3 °F	h B.t.u./hr. ft.^{2} °F
6.883	682	681	689	100.6
6.073	611	611	611	99.4
5.398	505	504	507	106.8
*4.732	341	344	344	137

*Unstable Film Point

APPENDIX B

SAMPLE CALCULATIONS

A. Sample Calculations for the First Data Point of Run 1

Data: $E = 2.5$ volts

$I = 10.0$ amperes

$\Delta T = 3.9°F$

$A = 4.0472(10)^{-2}$ ft^2

1. Calculation of the heat flux

$Q/A = (3.413EI)/A = 0.211(10)^4$ B.t.u./hr. ft.^{2}

2. Calculation of the heat transfer coefficient

$h = Q/(A\ \Delta T) = 541$ B.t.u./hr. ft.^{2}

B. Sample Calculations for the Critical Temperature Difference of Run 1

Data: $\Delta T_{bo} = 11.6°F$ from extrapolation of curve shown in Figure 6

$\Delta T_{vw} = 54.5°F$ from reference 19

ΔT_{bo} at $P_r=0.1 = 9.6°F$ from Figure 12

1. Calculation of ϵ

$\epsilon = \Delta T_{max}/\Delta T_{vw} = 0.21$

C. Sample Calculations for the First Data Point of Run 17

Data: $h = 41.3$ B.t.u./hr. ft.^{2} °F

$T_s = 139°R$

$\Delta T = 364°R$

$T_{ave} = 321°R$

$\rho_L = 50.5$ lb./ft.^{3} from reference 46

$\rho_v = 0.12$ lb./ft.^{3} from reference 46

$\sigma = 69.9(10)^{-5}$ #/ft. from Appendix F

$K_v = 9.2(10)^{-3}$ B.t.u./hr. °F ft. from Appendix F

$\mu_v = 2.84(10)^{-2}$ lb./ft. sec. from Appendix F

$L = 85.5$ B.t.u./lb. from references 38 and 46

$C_{pv} = 0.25$ B.t.u./lb. °F from reference 38

1. Calculation of λ_c

$$\lambda_c = 2\pi[(g_c\ \sigma)/g(\rho_L - \rho_v)]^{1/2} = 2.33(10)^{-2} \text{ ft.}$$

2. Calculation of F

$$F = [K_v^3\ \rho_v(\rho_L - \rho_v)gL(1 + \{0.34C_{pv}\ \Delta T\}/L)^2]^{1/4}$$

$$= 12.6$$

3. Calculation of $(h\ \lambda_c)/F$

$$(h\ \lambda_c)/F = 1.28$$

APPENDIX C

DISCUSSION OF THE EFFECT OF END LOSSES FROM THE HEAT TRANSFER ELEMENT

The magnitude of the axial temperature gradient for a heat transfer element similar to the one used in this investigation was measured in the preliminary work. The values of the temperature difference at given heat fluxes are given in Table C-1.

If the equation $q = - KA \frac{dT}{dx}$ is assumed to hold in the form $q = - KA \frac{\Delta T}{\Delta x}$, the heat losses from the element can be quickly calculated. The magnitude of the heat losses and the percentage of input heat which is lost is given in Table C-II. A thermal conductivity of 225 B.t.u./hr. ft.^{2} was assumed.

The magnitude of the end losses which occurred from the heat transfer element were of primary concern in the design of the heat transfer element. Since Banchero, Baker, and Boll (1) report that axial temperature gradients were "virtually eliminated" in their heat transfer element by using a copper cylinder 2 inches in length and 0.75 inches in diameter, the dimensions of the element used in this investigation were kept as close to those of Banchero as possible without introducing extreme fabrication problems. The final dimensions chosen for the heat transfer element are 2.3125 inches in length and 0.8022 inches in diameter. The diameter to length ratio of the element is 0.347 compared to a value of 0.375 for Banchero's element. Therefore temperature gradients at least as small as Banchero's can be expected.

Table C-I

$Q/A\ (10)^{-4}$ B.t.u./hr. ft.^{2}	(Temp. center − Temp. 1/4 inch from end) °F	region
0.278	0.0	nucleate
0.442	0.3	nucleate
3.96	1.0	burnout
0.44	0.6	film
1.30	2.0	film
2.85	2.0	film

Table C-II

$Q/A\ (10)^{-4}$ B.t.u./hr. ft.^{2}	Heat Input B.t.u./hr.	Heat Loss B.t.u./hr.	Per cent Heat Loss Rounded to High Per cent
0.278	112.5	0	0
0.442	179.6	3.8	2
3.96	1602.6	12.6	1
0.44	178.1	7.5	5
1.30	526.0	25.3	5
2.85	1153.4	25.3	2

APPENDIX D

CALIBRATION OF THERMOCOUPLES

The thermocouples used in this investigation were calibrated with a platinum resistance thermometer. The resistance of the thermometer was determined by using the potentiometer method described by Scott (51). Temperature differences were measured by placing the reference junction in liquid nitrogen and the heat transfer element in room air, a dry ice acetone bath, and liquid nitrogen. The values obtained with the resistance thermometer allowed the thermocouples deviation from standard tables (N.B.S. Circular 561) to be calculated. The millivolt deviation obtained for the thermocouples is given in Table D-1.

TABLE D-I

Deviation of Thermocouples from Standard Tables

Temperature °C	Deviation Millivolts
-196.18	0.000
- 79.40	0.022
- 25.17	0.034

APPENDIX E

CALIBRATION CURVE FOR PRESSURE GAUGE

TABLE E-I

CALIBRATION OF HEISE H15379 PRESSURE GAUGE

Gauge graduated in one pound per square inch increments of from 0 to 1000 pounds per square inch gauge. Gauge calibrated with an Ashcroft Gauge tester, type 1300.

Test Pressure P.S.I.G.	Gauge Reading P.S.I.G.
10	10
20	20
40	40
60	60
85	85
105	105
124.5	125
144.5	145
164.5	165
184.5	185
204.5	205
225	225
250	250
274.5	275
304.5	305
324.5	325
349.5	350
374.5	375
405	405
424.5	425
449.5	450
474.5	475
499.5	500

APPENDIX F

CALCULATED PHYSICAL PROPERTIES

TABLE I-F N_2 SURFACE TENSION

TABLE II-F CH_4 SURFACE TENSION

TABLE III-F N_2 THERMAL CONDUCTIVITY

TABLE IV-F CH_4 THERMAL CONDUCTIVITY

TABLE V-F N_2 VISCOSITY

TABLE VI-F CH_4 VISCOSITY

The methods which were used to calculate surface tension, vapor viscosity, and vapor thermal conductivity for methane and nitrogen are discussed below. The calculated values for the physical properties are given in Tables I-F through V-F.

Surface tension data for methane and nitrogen were calculated by extrapolation of low pressure data (29). The McLeod equation was used for the extrapolation as suggested by Prutton and Maron (47).

The thermal conductivity values for methane and nitrogen were calculated using the method suggested by Owens and Thodos (44,45).

The viscosity data for methane and nitrogen were calculated by extrapolation of the low pressure data of Johnston and McCloskey (30) for nitrogen and calculated low pressure data (52) for methane using the method suggested by Jossi, Stiel, and Thodos (32).

TABLE F-I

SURFACE TENSION FOR SATURATED LIQUID NITROGEN

Temperature °R	Surface Tension $(10)^{-5}$ lb./ft.
171	33.8
180	27.4
189	20.1
198	14.5
207	8.5
216	3.7
225	0.3
227	0

TABLE F-II

SURFACE TENSION FOR SATURATED LIQUID METHANE

Temperature °R	Surface Tension $(10)^{-5}$ lb./ft.
220	81.8
240	66.0
260	52.0
280	35.0
300	20.2
320	12.0
340	0.5
344	0

TABLE F-III

THERMAL CONDUCTIVITY OF NITROGEN VAPOR

K in B.t.u./hr. ft. °F

Temperature	Pressure P.S.I.A. 14.5	64	114	148	214	299	389	442	492	514	614	719	814
136	.0042	--											
159	.0050	--											
182	.0055	.0061	.0065	.0071									
204	.0062	.0067	.0071	.0076	.0080	.0100							
227	.0067	.0074	.0076	.0080	.0084	.0092	.0113	.0130	.0147	.0147	.0315	.0346	.0357
272	.0071	.0084	.0088	.0090	.0094	.0099	.0105	.0113	.0116	.0116	.0130	.0143	.0155
340	.0099	.0103	.0105	.0105	.0113	.0113	.0116	.0120	.0122	.0122	.0128	.0134	.0139
386	.0109	.109	.0166	.0116	.0120	.0120	.0126	.0126	.0130	.0130	.0134	.0139	.0143
454	.0126	.0126	.0132	.0132	.0134	.0134	.0139	.0139	.0141	.0141	.0151	.0151	.0151
568	.0151	.0151	.0155	.0155	.0155	.0155	.0160	.0160	.0164	.0164	.0168	.0168	.0168
681	.0176	.0176	.0176	.0176	.0176	.0176	.0176	.0176	.0181	.0181	.0185	.0185	.0185
908	.0218	.0218	.0218	.0218	.0218	.0218	.0218	.0218	.0255	.0225	.0231	.0231	.0231

TABLE F-IV

THERMAL CONDUCTIVITY OF METHANE VAPOR

K in B.t.u./hr. ft. °F

Temperature °R	Pressure P.S.I.A. 24	114	214	314	414	514	564	664	714	764	814	864
791	.0322	.0322	.0322	.0322	.0322	.0322	.0337	.0337	.0337	.0337	.0352	.0352
688	.0264	.0264	.0264	.0264	.0264	.0264	.0264	.0264	.0278	.0278	.0278	.0278
619	.0223	.0223	.0223	.0223	.0234	.0234	.0234	.0234	.0243	.0243	.0246	.0246
550	.0202	.0202	.0202	.0202	.022	.022	.022	.022	.022	.022	.0223	.0233
482	.0176	.0176	.0182	.0182	.0186	.0188	.0188	.0193	.0193	.202	.0202	.0202
447	.0158	.0158	.0167	.0167	.0176	.0182	.0182	.190	.190	.190	.199	.199
413	.0146	.0146	.0158	.0158	.0167	.0176	.0176	.0182	.0182	.0188	.0202	.0202
378	.0135	.0138	.0144	.0149	.0155	.0167	.0167	.0182	.0182	.0188	.0214	.0214
344	.0120	.0123	.0132	.0141	.0149	.0164	.0164	.0205	.0205	.0264	.0439	.0439
327	.0114	.0117	.0126	.0135	.0149	.0170	.0170					
310	.0108	.0111	.0123	.0129								
292	.0102	.0108	.0117									
275	.097	.0102										
258	.091	.100										
241	.085											
206	.0073											

TABLE F-V

VISCOSITY OF NITROGEN VAPOR

μ in Centipoises $(10)^{-5}$

Pressure P.S.I.A.	Temperature °R								
	180	198	216	252	270	306	360	450	540
14.5	697.5	763.1	826.4	948.4	1008.3	1125.3	1295.4	1554.7	1785.7
64	697.5	763.1	826.4	948.4	1008.3	1125.3	1295.4	1554.7	1785.7
114	741.7	801.2	860.8	976.7	1034.1	1147.7	1312.4	1569.7	1798.5
148		815.9	873.1	956.5	1042.7	1154.8	1320.0	1574.4	1801.9
214			907.5	1009.8	1061.1	1169.5	1331.3	1581.7	1809.0
299				1051.6	1094.3	1197.8	1349.4	1594.0	1817.6
389				1113.0	1131.1	1228.5	1371.6	1607.5	1827.0
442				1154.8	1160.6	1245.7	1383.9	1618.6	1821.3
478				1184.3	1182.7	1258.0	1393.7	1623.5	1838.5
514				1226.0	1207.3	1272.7	1403.5	1630.9	1843.4
614				1329.2	1231.9	1314.5	1433.0	1649.3	1871.7
719					1408.8	1375.9	1469.8	1672.6	1876.6
814					1585.7	1432.4	1506.7	1694.7	1915.9

TABLE F-VI

VISCOSITY OF METHANE VAPOR

μ in Centipoises $(10)^{-5}$

Temperature °R	Pressure P.S.I.A. 24	114	214	314	414	514	564	664	714	764	814	864
960	17.67	1774	1780	1781	1790	1797	1799	1806	1809	1813	1815	1821
860	16.05	1613	1619	1625	1631	1638	1642	1652	1655	1660	1663	1670
760	1444	1452	1460	1467	1474	1482	1488	1501	1505	1509	1513	1518
660	1293	1303	1310	1319	1328	1345	1349	1361	1364	1369	1379	1383
560	1142.0	1154	1164	1174	1188	1202	1213	1232	1215	1245	1254	1260
460	971.0	985	997	1014	1036	1051	1059	1083	1100	1113	1139	1156
360	777.8	796	812.3	842	883	898.5	918	954.5	972	993		
344.2	744.0	764	783	815	862	921	970	1412				
300	634.0	677										